frontiers | Frontiers in Built Environment

ORIGINAL RESEARCH
published: 14 April 2022
doi: 10.3389/fbuil.2022.856380

Optimized Strengthening Based on Concrete Jacketing for Minimum Eccentricity

Chara Ch. Mitropoulou[1], *Iordanis A. Naziris*[1,2], *Nikos Ath. Kallioras*[1] *and Nikos D. Lagaros*[1]*

[1]*Institute of Structural Analysis and Antiseismic Research, School of Civil Engineering, National Technical University of Athens, Athens, Greece,* [2]*Special Service of European Union Structural Funds for the Ministry of Maritime Affairs and Insular Policy, Piraeus, Greece*

The coupled lateral-torsional response is observed in building structures subjected to dynamic excitation due to lack of symmetry in terms of mass/stiffness in any of the stories' plan views; such structural systems are called eccentric. Much damage and even collapse are concerned with building structures with asymmetric plan views. Combined torsional-translational vibration of their structural system results in higher ductility demands, especially to vertical structural elements located at the perimeter of the plan view. This study examines the minimization problem of the torsional response of an eccentric, multi-story reinforced concrete (RC) building by strengthening its vertical structural elements with RC jackets. The problem of minimizing the eccentricity between mass and rigidity centers for all story layouts and the corresponding minimization problem of the eccentricity between mass and strength centers for all stories are considered two separate formulations for the reduction of the torsional response optimization problem. Based on recent studies, the center of strength is preferable for assessing the torsional response of buildings in case of inelastic response. The imperialist competitive algorithm (ICA), a member of the family of evolutionary search algorithms, is used to solve the two optimization problems. The optimization problems are formulated for the case study building considered after assessing its structural behavior and capacity through nonlinear static analyses before and after strengthening. The later process was implemented to meet code requirements and examine the improvements achieved through optimization.

Keywords: strength eccentricity, stiffness eccentricity, metaheuristics, column strengthening, concrete jacketing, optimization

OPEN ACCESS

Edited by:
Vagelis Plevris,
Qatar University, Qatar

Reviewed by:
Michele Palermo,
University of Bologna, Italy
Rajai Zuheir Al Rousan,
Jordan University of Science and Technology, Jordan
Sameh Samir F. Mehanny,
Cairo University, Egypt

***Correspondence:**
Nikos D. Lagaros
nlagaros@central.ntua.gr

Specialty section:
This article was submitted to Computational Methods in Structural Engineering, a section of the journal Frontiers in Built Environment

Received: *17 January 2022*
Accepted: *09 March 2022*
Published: *14 April 2022*

Citation:
Mitropoulou CC, Naziris IA, Kallioras NA and Lagaros ND (2022) Optimized Strengthening Based on Concrete Jacketing for Minimum Eccentricity. Front. Built Environ. 8:856380. doi: 10.3389/fbuil.2022.856380

1 INTRODUCTION

During the structural design phase, which remains the subject of research for engineers and scientists, the goal is to develop a structural system that can reliably and predictably withstand dynamic excitation (i.e., due to extreme actions such as blast loading or seismic excitation). Coupling translational with torsional response can be observed due to either variance between actual and considered mass distribution and stiffness or dynamic excitations that introduce a torsional component on the structural response. This component is developed due to eccentricity between the centers of mass (CM) and rigidity (CR) of the structural system. Such a structural system is called eccentric or torsionally unbalanced. When this kind of structural system is subject to horizontal dynamic excitations, the inertia forces developed can be represented by point loads passing through

the mass center, while the forces modeling the resisting extreme action can be represented as point loads passing through the stiffness center. This pair of opposing point loads generates the torsional component of the response on the structural system coupled with the translational one.

It is worth mentioning that the foundations of modern research on the dynamic behavior of single and multi-story asymmetric structures were set by a series of studies that identified some of the key parameters influencing the performance of such systems. For instance, Goel and Chopra (1990) and Kan and Chopra (1977) identified and assessed the distribution of stiffness and strength and the torsional coupling, respectively. Further influential studies regarding the response of one-story structures are included in the works of Peruš and Fajfar (2005), Palermo et al. (2013), Palermo et al. (2017), and Trombetti and Conte (2005). Additionally, Fajfar (2000) and Fischinger (Fajfar and Fischinger, 1988; Fajfar and Gašperšič, 1996; Marušić and Fajfar, 2005) analyzed the nonlinear response of multi-story buildings under seismic loads. Bosco et al. (2012), Bosco et al. (2013), Bosco et al. (2015) also approached the behavior of multi-story asymmetric buildings, while De Stefano and Pintucchi (2008) presented a useful overview of the research advancements about the seismic response of both the plan and vertically irregular structures.

As proved by Kan and Chopra (1977) and presented in more detail by Reem and Chopra (1987), accurate and reliable prediction and assessment of the response of eccentric multi-story buildings in the elastic stage cannot be determined because, in multi-story buildings, except in a special case, the center of rigidity is not defined unambiguously but depends on seismic loading. Eurocode 8 (1994) and its Greek national annex provided the definition of a fictitious axis of rotation (optimum torsion axis) from which static eccentricity is measured. Regarding the post-elastic structural response stage, things are even vaguer. For example, Stathopoulos and Anagnostopoulos (2005) questioned the adoption of a single coefficient of behavior q provided by modern earthquake design provisions. However, during the past 30 years, research efforts were performed in this direction (estimating and predicting the response of eccentric buildings), and various design criteria/estimation of torsional action have been proposed (Stathi et al., 2015).

In buildings designed with older regulations (before 1995 and especially before 1985), significant non-uniformities are observed during the formation of the static system. On the contrary, new buildings are characterized by greater regularity, thanks to the provisions of modern earthquake design codes (Anastassiadis et al., 1998; Makarios and Anastassiadis, 1998; Xenidis et al., 2006). Modern earthquake design codes try to provide general directions (simple as possible structural systems, arrangement of strong stiffness elements in the perimeter, etc.), aiming to derive as rigid as possible buildings but also with limitations in terms of geometry and distribution of stiffness and mass along the height and floor plans. However, in relevant provisions based on simplified shear-beam, one-story models, the "flexible" side frames exhibit higher ductility demands than the "stiff" side ones (Stathopoulos and Anagnostopoulos, 2005). The advancements of computational techniques and algorithms have allowed scientists in several fields to approach multiple complex problems in new and efficient ways. Particularly in engineering, such techniques have significantly contributed to the shift from traditional trial-and-error practices to fully automated ones, incorporating search algorithms. There are many examples from the past where researchers have explored the potential of implementing optimization approaches to structural engineering challenges. Furthermore, the behavior of asymmetric structures subjected to horizontal loads, such as earthquakes, especially regarding their torsional response, is addressed in numerous research studies, which in some cases also incorporate optimization approaches to solve the arising problems.

Specifically, Terzi and Athanatopoulou (2021) proposed a measure to define the optimum torsion axis through the twist axis. This measure demands the sum of story translational displacements of the axis to be minimal. Dang et al. (2021) developed a two-stage optimization approach for designing isolated buildings incorporating genetic algorithms to identify the optimal parameters of the isolated layer. Almazán and de la Llera (2009) showed that the optimal damper location depends on the static eccentricity and frequency ratio of the bare structure, the total amount of supplemental damping considered, and the frequency content of the excitation. Li and Han (2003) optimized the positioning of multiple tuned mass dampers (MTMD) for asymmetric structures, while Ismail (2015) aimed at forcing the isolated asymmetric structures to behave as symmetric structures, eliminating torsional responses. Similarly, Georgoussis (2015) suggested a way to minimize the torsional response of inelastic multi-story buildings with simple eccentricity, and Yiu et al. (2014) introduced a practical method for evaluating lateral-torsional coupling in the elastic earthquake response of asymmetric multi-story buildings. In order to minimize the torsional effects in asymmetric tall buildings, Şahin (2012) proposed a new algorithm in MATLAB. Lagaros et al., in two studies (2006 and 2009), developed optimum design approaches for improving the seismic performance of 3D RC buildings, including the minimization of the rigidity eccentricity. In the same context, Duan and Chandler (1997) developed an optimized procedure for designing torsionally unbalanced structures subjected to earthquake loading, considering both the serviceability and the ultimate limit states. Three studies (Li et al., 2008a; Li et al., 2008b; Li et al., 2008c) extensively dealt with the properties of soil-asymmetric building-active multiple tuned mass dampers (AMTMD) interaction system, suggesting guidelines for the design and implementation in earthquake reduction of asymmetric structures built on soft soil foundation. Guo and Li (2009) established a model of primary-secondary systems concerning lateral-torsion coupling and interaction between primary and secondary systems and used a complex mode theory and pattern research method for the secondary system's optimal position. They also analyzed the influencing factors of optimal position, such as eccentricity of the primary system, direction of earthquake input, site of different classification, mass, frequency, and damping ratio of the secondary system. Chandler et al. (1995) examined the

influence of accidental eccentricity on inelastic seismic torsional effects in buildings reaching some useful conclusions regarding the effectiveness of code accidental torsional provisions and the ductility demand for the flexible-edge element in torsionally unbalanced structures. Finally, Etedali and Kareshk (2022) proposed a procedure for the optimal design of isolators in the base story of asymmetric base-isolated structures to mitigate torsional responses. In this work, the minimum eccentricity optimization problem is formulated for the case of multi-story reinforced concrete (RC) building structures associated with the problem of selecting the characteristics of their vertical structural elements strengthening strategy. In order to offer the designer/practitioner a tool to understand the procedures described in the study, an open-access web application is provided, where optimization-based strengthening is provided, among others (LINK).

2 ECCENTRICITY IN MULTI-STORY BUILDING STRUCTURES

2.1 Equations of Motion

Contrary to what is observed for the case of single-story building structures, in the case of multi-story ones, the centers of mass, rigidity, and strength do not lie over a vertical axis. Another difference observed in the case of multi-story buildings is that the locations of the centers of stiffness, twist, and shear depend on the stiffness of the system and the torsional or lateral loads exerted. However, a special type of multi-story buildings can be designed where, in each story, these centers coincide, laying over a common, vertical axis independent of lateral loading. The typical centers that can be defined for each story of the multi-story building are the following: stiffness center (also called rigidity center) is the location on each floor where any set of static horizontal forces of arbitrary magnitude and direction is applied to cause no rotation or twisting on any of the stories (Hejal and Chopra, 1989). Another definition of the stiffness center of a building is that it corresponds to the location on each floor where if a static horizontal force is applied, it develops translational deformation without rotation or twisting. However, the rest of the floors may rotate or twist (Humar, 1984). The principal axes of a floor are two orthogonal axes passing through its center of rigidity. If a set of static horizontal loads is applied along one of the two principal axes of each floor, then the floor is deformed along the direction of the applied loads, without a twist. The mass center is the location on the diaphragm where the component of the inertial forces of the floor passes. If the masses of the vertical elements are negligible compared to those of the floor and the mass distribution on the floors of the building is uniform, then the center of mass coincides with the geometric center of the floor. The static eccentricity of the ith story refers to the distance between mass and stiffness centers.

The equations of motion of a multi-story building, considering linear behavior, where damping is ignored for simplicity in the description, for the case of a dynamic action along the x- and y-axis, developing accelerations $a_{gx}(t)$ and $a_{gy}(t)$, respectively, are formulated as follows for various reference points. With reference to a randomly selected reference point O,

$$\begin{bmatrix} m & 0 & -my_{CM} \\ 0 & m & mx_{CM} \\ -my_{CM} & mx_{CM} & J_0 \end{bmatrix} \begin{Bmatrix} \ddot{u}_x \\ \ddot{u}_y \\ \ddot{u}_\theta \end{Bmatrix} + \begin{bmatrix} K_x & K_{xy} & K_{x\theta} \\ K_{yx} & K_y & K_{y\theta} \\ K_{\theta x} & K_{\theta y} & K_\theta \end{bmatrix} \begin{Bmatrix} u_x \\ u_y \\ u_\theta \end{Bmatrix} = -\begin{Bmatrix} mIa_{gx}(t) \\ mIa_{gy}(t) \\ -y_{CM}mIa_{gx}(t) + x_{CM}mIa_{gy}(t) \end{Bmatrix}, \tag{1}$$

with reference to the center of mass CM,

$$\begin{bmatrix} m & 0 & 0 \\ 0 & m & 0 \\ 0 & 0 & J_M \end{bmatrix} \begin{Bmatrix} \ddot{u}_x \\ \ddot{u}_y \\ \ddot{u}_\theta \end{Bmatrix} + \begin{bmatrix} K_x & K_{xy} & K_{x\theta} \\ K_{yx} & K_y & K_{y\theta} \\ K_{\theta x} & K_{\theta y} & K_\theta \end{bmatrix} \begin{Bmatrix} u_x \\ u_y \\ u_\theta \end{Bmatrix} = -\begin{Bmatrix} mIa_{gx}(t) \\ mIa_{gy}(t) \\ 0 \end{Bmatrix}, \tag{2}$$

with reference to the rigidity center CR,

$$\begin{bmatrix} m & 0 & -me_y \\ 0 & m & me_x \\ -me_y & me_x & J_R \end{bmatrix} \begin{Bmatrix} \ddot{\tilde{u}}_x \\ \ddot{\tilde{u}}_y \\ \ddot{u}_\theta \end{Bmatrix} + \begin{bmatrix} \tilde{K}_x & \tilde{K}_{xy} & 0 \\ \tilde{K}_{yx} & \tilde{K}_y & 0 \\ 0 & 0 & \tilde{K}_\theta \end{bmatrix} \begin{Bmatrix} \tilde{u}_x \\ \tilde{u}_y \\ u_\theta \end{Bmatrix} = -\begin{Bmatrix} mIa_{gx}(t) \\ m1a_{gy}(t) \\ -e_y m1a_{gx}(t) + e_x m1a_{gy}(t) \end{Bmatrix}, \tag{3}$$

where I denotes a vector of ones of dimension N; $\ddot{u}_x$, $\ddot{u}_y$, and $\ddot{u}_\theta$ denote vectors of dimension N; J_0 is the diagonal matrix of dimension N (number of stories in a multi-story building structure) and its elements $J_{0,j}$ denote the polar moment of inertia of the j^{th} story with respect to point O_j; r is the radius of rotation; x_{CM} and y_{CM} are diagonal matrices of dimension N and their elements $x_{CM,j}$ and $y_{CM,j}$ denote the coordinates of the mass center (CM) of the j^{th} story with respect to the reference system $X_jO_jY_j$; J_M is the diagonal matrix of dimension N where its elements $J_{M,j} = m_j r_j^2$ represent the polar moment of inertia of the j^{th} story with reference to its mass center; J_R denotes the diagonal matrix of dimension N and its elements $J_{R,j} = m_j(e_j^2 + r_j^2)$ denote the polar moment of inertia of the j^{th} story with respect to the center of stiffness; and e_x and e_y are diagonal matrices of dimension N and their elements are defined as follows:

$$e_{xj} = x_{CMj} - x_{CRj}, \tag{4a}$$

$$e_{yj} = y_{CMj} - y_{CRj}, \tag{4b}$$

where scalars e_{xj} and e_{yj} are the components of the static eccentricity of the j^{th} story along the x- and y-axis and x_{CRj} and y_{CRj} are coordinates of the stiffness center of the j^{th} story with respect to the reference system $X_jO_jY_j$.

2.2 Location of Stiffness or Rigidity Center

To calculate the coordinates of the stiffness center (also called rigidity center) for the case of a multi-story building structure, let us consider the stiffness matrix of **Eq. 1**, which is defined

according to degrees of freedom (DOF) u at a randomly selected reference point O. Hence, for calculating the coordinates, the following transformation of u (corresponding to reference point O) to $\tilde{u}$ (corresponding to reference point CR) is considered:

$$u = \begin{Bmatrix} u_x \\ u_y \\ u_\theta \end{Bmatrix} = \begin{bmatrix} I & 0 & y_{CR} \\ 0 & I & -x_{CR} \\ 0 & 0 & I \end{bmatrix} \begin{Bmatrix} \tilde{u} \\ \tilde{u} \\ u_\theta \end{Bmatrix} = \tilde{a}\tilde{u}. \tag{5}$$

Thus,

$$\tilde{\mathrm{K}} = \tilde{a}^T K \tilde{a} \Leftrightarrow \tilde{\mathrm{K}} = \begin{bmatrix} K_x & K_{xy} & K_x y_{CR} - K_{xy} x_{CR} + K_{x\theta} \\ K_{yx} & K_y & K_{yx} y_{CR} - K_y x_{CR} + K_{y\theta} \\ K_{\theta x} + y_{CR} K_x - x_{CR} K_{yx} & K_{\theta y} + y_{CR} K_{xy} - x_{CR} K_y & \tilde{K}_\theta \end{bmatrix}, \tag{6}$$

where $\tilde{K}_\theta = K_\theta + 2K_{\theta x} y_{CR} - 2K_{\theta y} x_{CR} + K_x y_{CR}^2 - 2K_{xy} x_{CR} y_{CR} + K_y x_{CR}^2$, given that **Eq. 6** refers to the stiffness matrix with reference to CR, and as denoted in **Eq. 3**, the off-diagonal coefficients of the stiffness matrix that correspond to the coupling of translational with rotational DOF are equal to zero:

$$K_{\theta x} + y_{CR} K_x - x_{CR} K_{yx} = 0, \tag{7a}$$

$$K_{\theta y} + y_{CR} K_{xy} - x_{CR} K_y = 0, \tag{7b}$$

Thus, solving the system of **Eq. 7a**, **Eq. 7b**, with respect to the unknowns x_{CR} and y_{CR} that denote diagonal matrices containing the coordinates of the rigidity centers along the stories of the building structure and their coefficients ($K_{\theta x}$, K_x, etc.,) referring to square matrices, the following expressions are derived:

$$x_{CR} = \frac{K_{y\theta} - K_{yx} K_x^{-1} K_{x\theta}}{K_y - K_{yx} K_x^{-1} K_{xy}}, \tag{8a}$$

$$y_{CR} = -\frac{K_{x\theta} - K_{xy} K_y^{-1} K_{y\theta}}{K_x - K_{xy} K_y^{-1} K_{yx}}. \tag{8b}$$

However, **Eq. 8a**, **Eq. 8b** do not always lead to diagonal matrices, thus unique definition of the centers of stiffness. Unique locations of stiffness centers do not always exist. They depend on loading; that is, different load distributions lead to different locations of the stiffness centers. In such a case, the coordinates of the stiffness centers can be derived through the following procedure:

$$\tilde{P} = \tilde{K}\tilde{u} \Leftrightarrow \begin{Bmatrix} \widetilde{P_x} \\ \widetilde{P_y} \\ 0 \end{Bmatrix} = \begin{bmatrix} K_x & K_{xy} & K_x y_{CR} - K_{xy} x_{CR} + K_{x\theta} \\ K_{yx} & K_y & K_{yx} y_{CR} - K_y x_{CR} + K_{y\theta} \\ K_{\theta x} + y_{CR} K_x - x_{CR} K_{yx} & K_{\theta y} + y_{CR} K_{xy} - x_{CR} K_y & \tilde{K}_\theta \end{bmatrix} \begin{Bmatrix} \tilde{u}_x \\ \tilde{u}_y \\ u_\theta \end{Bmatrix}, \tag{9}$$

where static lateral loads are introduced along the height of the building structure, leading to the following expressions:

$$x_{CR} = \left[\widetilde{P_y}\right]^{-1} \frac{K_{\theta y} - K_{\theta x} K_x^{-1} K_{xy}}{K_y - K_{yx} K_x^{-1} K_{xy}} \widetilde{P_y}, \tag{10a}$$

$$y_{CR} = -\left[\widetilde{P_x}\right]^{-1} \frac{K_{\theta x} - K_{\theta y} K_y^{-1} K_{yx}}{K_x - K_{xy} K_y^{-1} K_{yx}} \widetilde{P_x}, \tag{10b}$$

where $\widetilde{P_x}$ and $\widetilde{P_y}$ are diagonal matrices. Therefore, the location of the stiffness centers is unique and dependent on the applied load. It is possible to identify unique stiffness centers along the floors of multi-story building structures, regardless of the horizontal loads, for a special type of multi-story buildings that allows the identification of unique centers and has the following properties: 1) the mass centers of all floors lie along a vertical axis and 2) the vertical structural elements are arranged in such a way that their local axes form an orthogonal grid in the floor plan view and are connected to each floor by a rigid diaphragm. The result of the last two characteristics is that the stiffness centers of all floors are on the same vertical axis. The static eccentricities of the floors are also the same (Lagaros et al., 2006; Lagaros et al., 2009).

2.3 Location of Strength Center

As mentioned earlier, the regulations are based on an elastic response; the simulation of the torsional effect, however, needs to consider the inelastic state of the body (determination of the torsional axis in the inelastic phase, ability to receive the shear forces of torsion from the structural elements) that will determine the collapse mechanisms of the building and thus give the ability to the engineer to estimate the required ductility of the components and compare it with the available one. There are many relevant ones in the literature (e.g., Stathopoulos and Anagnostopoulos, 2005). It has been proposed to replace the rigidity center (CR) with that of the strength center (CV). The center of strength (CV) is the position of the diaphragm through which the recommended strength of all vertical elements passes. Strictly unrestrained is a building whose mass and stiffness centers are not identical (eccentric) (Paulay, 1998; Penelis and Penelis, 2019). According to the above, the CV endurance center is determined as follows:

$$x_{CV} = \frac{\Sigma_i V_{yi} \cdot x_i}{\Sigma_i V_{yi}}, \tag{11a}$$

$$y_{CV} = \frac{\sum_i V_{xi} \cdot y}{\sum_i V_{xi}}, \tag{11b}$$

where x_i and y_i are the coordinates of the vertical elements' center of mass of the ith story with respect to the typical reference system on the specific story, V_{xi} and V_{yi} denote the horizontal (shear) nominal resistance (strength) of the vertical elements along the directions x and y, respectively, which are calculated in case of a fragile element:

$$V_y = min\left\{\frac{M_x}{L_{s,k}}; V_{Ry}\right\}, \tag{12a}$$

$$V_x = min\left\{\frac{M_y}{L_{s,k}}; V_{Rx}\right\}, \tag{12b}$$

with $L_{s,k}$ denoting the distance of the extreme cross section $k = 1$, 2 of the specific element from the position of zero moments (shear length), where the shear strength of the element along the

two directions (V_{Ry} and V_{Rx}) is calculated based on appendix 7Γ of Kanepe (2017).

3 STRENGTHENING OF RC BUILDING STRUCTURES

Several options are available for intervention aiming to retrofit structures (Costa et al., 2017; Ganguly, 2020). 1) Repair–reinforcement of critical areas on existing structural elements: jacketing is the most popular method of this category, contributing to strengthening and retrofitting structural elements. It is adopted to upgrade bearing load capacity based on improvements on the structural design or restore its integrity due to failures on the structural elements (steel jacketing, reinforced concrete jacketing, glass fiber reinforced polymer jacketing, fiber-reinforced polymer (FRP) jacketing, hybrid jacketing and shape memory alloy (SMA) wire jacketing, near-surface mounted (NSM) fiber-reinforced polymer (FRP) jacketing, etc.). 2) Add new load-bearing elements (new structural system, shear walls, steel frame, etc.): filling shear walls of the load-bearing frame structural system, expansion (reinforcement of existing brickwork, demolition of brickwork and addition of RC shear walls, steel stiffeners/dampers). 3) Addition of dampers: seismic isolation systems. All the above-mentioned options are part of a structural intervention strategy.

3.1 Structural Intervention Aiming to Remove Irregularities in the Floor Plan

In order to choose how and where to intervene in the building aiming to improve its structural performance is to increase stiffness and flexural strength of some structural elements selectively, for example, for the case of columns aiming to modify the location of the centers of elastic stiffness and strength and possibly minimize the corresponding eccentricities. According to Tassios (1982), a selective increase in stiffness takes place 1) after low-intensity random actions (e.g., low-intensity explosions and small earthquakes), 2) when the building is very flexible, and 3) when it is necessary to correct irregularities in the distribution of stiffness in height or extent. Selective increase of flexural strength occurs due to 1) irregularity of strengths in height or plan (i.e., torsion might be observed during yield of some elements) and 2) insufficiency of flexural strength locally or damage of a structural element. Such problems require a selective increase in stiffness and flexural strength of the columns. The most suitable strengthening method is the use of reinforced concrete jacketing (Kanepe, 2017).

3.2 Column Jacketing

The construction of jackets on RC columns is a repair and reinforcement method successfully applied in numerous cases. The method is used to repair or strengthen the element (local or total jacketing). In addition to improving the three basic features of the column, jacketing also does not affect the architectural characteristics of the strengthened section, reduces slenderness of the strengthened element, improves the structural performance of the columns due to confinement, and increases the level of fire protection. Based on the type of concrete, jacketing is classified into two different categories. Jacketing made of cast concrete is used in jackets where the thickness exceeds 8 cm ($t \geq 8$ cm), while their construction requires formwork. Casting is implemented by means of low pressure, and the size of the aggregates should not be large. The use of fluids and admixtures that prevent drying shrinkage is recommended. The disadvantages of this technique are the difficulty of concreting, especially at the top of the column. In cases where the total thickness is less than 10 cm ($t \leq 10$ cm), Jacketing made of sprayed/shot concrete is used, while no formwork is required for pouring or placing into them. Particular attention should be paid to ensuring the vertical surface of the jackets *via* guides usage. The drying shrinkage in this type of concrete jackets is greater. Thus, proper maintenance is required.

The construction provisions of RC jackets are the result of research and experience from the application of the method in practice: For sprayed/shot concrete jacketing, the minimum thickness must be 5 cm; for cast concrete jacketing with one row of reinforcements, the thickness must be 8–12 cm; and for cast concrete jacketing with two rows of reinforcement, the minimum thickness must be 12 cm. In the case where the thickness of the jacketing is small (i.e., less than 7.50 cm), the provisions of the concrete regulations related to the coatings of the reinforcement bars are not satisfied together with those related to the form of hooks at the ends of the stirrups. Thus, in case of a small thickness of the jacket, the ends of the stirrups need to be welded.

4 THE MINIMUM ECCENTRICITY PROBLEM COMBINED WITH COLUMNS STRENGTHENING FOR RC BUILDING STRUCTURES

4.1 Problem Formulation

The main objective of this study is to formulate optimization problems that will lead to the redesign of existing RC structures, which may have been reinforced to meet the required safety conditions of the applicable Regulations, in order to create designs with the minimal torsional response and therefore improved behavior. The wording used in this work is based on the problem of minimizing the e_{CM-CV} eccentricity of centers of mass (CM) and strength (CV) for each story. Design variables (in the case of existing buildings) are the thickness and the longitudinal reinforcement of the RC jackets. Restrictions refer to the value ranges in which these variables move due to construction and regulatory requirements. The problem refers to a mixed optimization problem mathematically expressed as follows:

$$\min_{[t]} e_{CM-CR}([t]) = \sqrt{\left(x^j_{CM}([t]) - x^j_{CR}([t])\right)^2 + \left(y^j_{CM}([t]) - y^j_{CR}([t])\right)^2},\ j = 1\,2,\ \cdots, n_{storeys}, \tag{13a}$$

$$\min_{[t,p]} e_{CM-CV}([t,p]) = \sqrt{\left(x^j_{CM}([t,p]) - x^j_{CV}([t,p])\right)^2 + \left(y^j_{CM}([t,p]) - y^j_{CV}([t,p])\right)^2},\ j = 1\,2,\ \cdots, n_{storeys}, \tag{13b}$$

where $[x^j_{CM}, y^j_{CM}]$, $[x^j_{CR}, y^j_{CR}]$, and $[x^j_{CV}, y^j_{CV}]$ are the positions of the mass, rigidity, and strength centers of the j^{th} story, $n_{storeys}$ is the total number of floors of the building, $t = [t_{NS}, t_S]$ are the RC jackets' thicknesses of the non-strengthened and strengthened (based on safety criteria) columns, respectively, $n_{columns,NS}$ and $n_{columns,S}$ denote the total number of non-strengthened and strengthened columns of the story, respectively, p denote the percentage of longitudinal reinforcement of the RC jackets, and $n_{columns} = n_{columns,NS} + n_{columns,S}$ is the total number of columns of the story.

The notations marked in **Figure 1** are the following: $t_{tot} = t_0 + t_{new}$ is the total thickness of the RC jacket resulting from the strength requirements plus the one needed to minimize eccentricity, $A_{s,ini,y}$ is the initial longitudinal reinforcement of the cross section, perpendicular to the y direction, and $A_{s,ini,x}$ is the initial longitudinal reinforcement of the cross section, perpendicular to X direction. Accordingly, $A_{s,tot} = A_{s,0} + A_{s,new}$ is the total reinforcement of the RC jacket resulting from the strength requirements plus the one needed to minimize eccentricity. In order to calculate the strength moment and the corresponding shear forces, the cross section is discretized into layers of number:

$$l_x = round\left[\frac{h + 2t_{tot}}{h_l}\right], // \, with\ direction\ x\,, \tag{14a}$$

$$l_y = round\left[\frac{b + 2t_{tot}}{h_l}\right], // \, with\ direction\ y, \tag{14b}$$

where h_l is the thickness of the layer, after trial-and-error tests, to achieve a compromise between convergence to acceptable results and velocity $h_l = 1.0\,cm$.

The following assumptions are considered for the implementation of the algorithm. First assumption: a common RC jacket is constructed with thickness $t_{tot} = t_0 + t_{new}$ and reinforcement lying on the same level as shown in **Figure 1**. Second assumption: in order to calculate the bending moment resistance, only the longitudinal reinforcement distributed along the edge of the cross section perpendicular to the specific direction is used because the contribution of the rest is rather limited. Third assumption: uniform distribution of the stresses over the layer thickness is considered equal to its upper limit. Fourth assumption: 3 cm reinforcement coating is considered for the initial cross section and RC jacket.

4.1.1 Calculation of the Objective Functions

The steps of the algorithm for calculating the rigidity eccentricity e_{CM-CR} for each floor are as follows, for each column and in each direction:

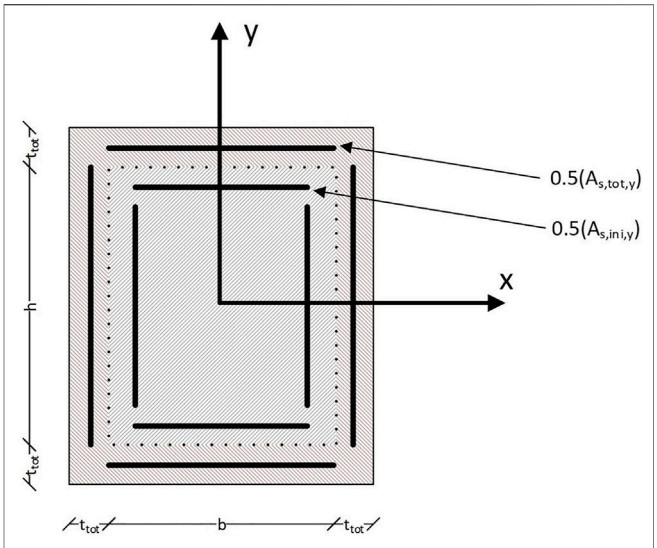

FIGURE 1 | Strengthening of RC cross section to calculate its resistance to axial bending with axial force.

Step 1: calculation of the moment of inertia along the directions of local axes x and y for each column by the method of the equivalent cross section.
Step 2: calculation of the cracked stiffness of the cross section for each column.
Step 3: calculation of CR stiffness center coordinates (for the pure frame or wall system).
Step 4: calculation of the objective function according to **Eq.13a**.

Accordingly, the steps of the algorithm for calculating the strength eccentricity e_{CM-CV} for each floor are as follows, for each column and in each direction:

Step 1: discretization of the cross section according to **Eq. 14b**, **Eq. 14a**.
Step 2: calculation of bending moment resistance for combined loading of bending and axial loading. Given that the element is considered monolithic, its strength was reduced by coefficient $k_r = 0.90$ according to KANEPE (Code of Structural Interventions).
Step 3: calculation of shear strength considering a bending failure according to **Eq. 12a**, **Eq. 12b**.

Then, given that the shear strength of the columns is available along the two principal axes, the following steps are performed:

Step 4: calculation of the coordinates of the center of resistance.
Step 5: calculation of the objective function according to **Eq.13b**.

4.1.2 Data Entry

In order to introduce the information required by the problem formulation, a common matrix of the input data is used [data (N,14)], where $N = n_{columns}$ is the number of columns in each story. The 14 columns of the matrix correspond to (c1) column dimension parallel to the x-axis [b (m)], (c2) column dimension

parallel to the y-axis [h (m)], (c3) initial mechanical percentage of reinforcement (p), (c4) abscissa of the column's section mass center [x (m)], (c5) ordinate of the column's section mass center [y (m)], (c6) stiffness reduction coefficient due to cracking, (c7) initial reinforcement thickness (element strength requirements), (m), (c8) mechanical reinforcement rate of initial reinforcement, (c9) additional reinforcement thickness resulting from minimizing construction eccentricity [t_{new} (m)], (c10) mechanical percentage of additional reinforcement (ρ_{new}), (c11) modulus of elasticity of concrete [E_c (kPa)], (c12) modulus of elasticity of steel reinforcement [E_s (kPa)], (c13) column length [L (m)], and (c14) axial compressive strength of concrete for the combination G + 0.3Q (with positive sign), [N (kN)].

4.2 Solving the Optimization Problem

Search algorithms represent an iterative procedure that requires an initial guess of the problem solution. Then, a sequence of improved designs are generated until the optimal or the best compromise solution is achieved. The type of strategy that the algorithm relies on for generating the new designs categorizes the optimization procedure. The search algorithm is characterized by robustness, in which the algorithm needs to be able to handle a variety of problems efficiently; efficiency, in which the algorithm should not require too much computing power to converge; and accuracy in which the algorithm needs to be able to recognize an acceptable solution accurately, without being sensitive to arithmetic errors.

A fast algorithm may require too much storage to deal with problems with many design variables. On the contrary, a highly robust algorithm may require many iterations, thus increasing computational time to reach the optimal design. Some algorithms preserve part of the information from the previous designs, while others only use information from the current design. As far as the type of information, the algorithms are classified into zero-, first-, or second-order algorithms. Zero-order algorithms use the information obtained through objective function value only during the search process. First-order algorithms, in addition to the objective function value, make use of the information obtained through the first-order derivative of the objective function. In contrast, second-order algorithms, in addition to the objective function value and its first derivative, use the information obtained through the second-order derivative of the objective function.

Zero-order algorithms are divided into deterministic or mathematical and stochastic algorithms, depending on how the new designs are generated. In general, deterministic ones approach the optimal design very quickly. Their main disadvantage is that they are easily trapped in local minima. Stochastic algorithms search for the optimal solution through random processes, generating better designs based on the existing ones. They are not as easily trapped into local minima as deterministic algorithms. They require much more computing power to converge. For many years, deterministic algorithms were the exclusive tool for solving structural design optimization problems. However, stochastic algorithms have been explored since the 1960s. During the last 2 decades, stochastic algorithms have been extensively applied in the field of structural design optimization at the research level and have managed to provide solutions to particularly demanding and complex problems. Search algorithms are also classified into algorithms that, in each iteration, deal with one design only and those that deal with a population of designs. All deterministic algorithms deal with one design in each iteration. Concerning the stochastic algorithms, simulated annealing is the most popular search algorithm that also deals with one design in each iteration.

A large and very popular category of stochastic search algorithms that deal with a population of designs in each iteration are the well-known evolutionary or Darwinian algorithms. They usually model a natural, social, or biological process. Evolutionary algorithms are characterized by robustness and the ability to identify the area of the global optimum design due to the random search process. However, they require a large number of function evaluations. Genetic algorithms and evolution strategies are the best-known evolutionary algorithms. For dealing with the optimization problems addressed in the framework of the IMSFARE project, the imperialist competitive algorithm (ICA) was employed, which is briefly described in the next section.

4.3 Imperial Competitive Algorithm

ICA (Atashpaz-Gargari and Lucas, 2007) is an evolutionary search algorithm inspired by imperialist competition. So far, it has been used successfully in different optimization problems of numerous areas of engineering and science. The independent populations are called countries and are of two types, colonies and imperialists, all of which together form empires. The colonial/imperialistic competition between empires is the basis of the algorithm. During this competition, the weak empires collapse while the strong ones take over the colonies of the weak empires. This competition successfully converges to the stage where there is only one empire after the collapse of all the rest, whose colonies are positioned in the same location with the imperialist, having the same cost (i.e., the same objective function value). From one point of view, ICA can be considered the social equivalent of genetic algorithms. ICA is the mathematical model and computational simulation of human social evolution, while genetic algorithms are based on the biological evolution of species. Subsequently, the steps of the algorithm and how the imperialist competition between empires is modeled is provided in more detail.

Step 1 (creation of initial empires): like any other evolutionary algorithm, ICA starts with a random initial population (countries in the world). Some of the countries are chosen to be the colonialists/imperialists and the rest form the colonies of these imperialists. These original colonies are divided among the imperialists according to their power, proportional to their cost. It should be mentioned that the cost of a country (design) refers to the objective function value. Let $p_1, p_2, \cdots p_n$ denote the design variables required to model the optimization problem at hand. Thus, a country is defined with the vector $country = [p_1, p_2, \cdots p_n]$. The design variables take various values randomly chosen over the design space, and thus the

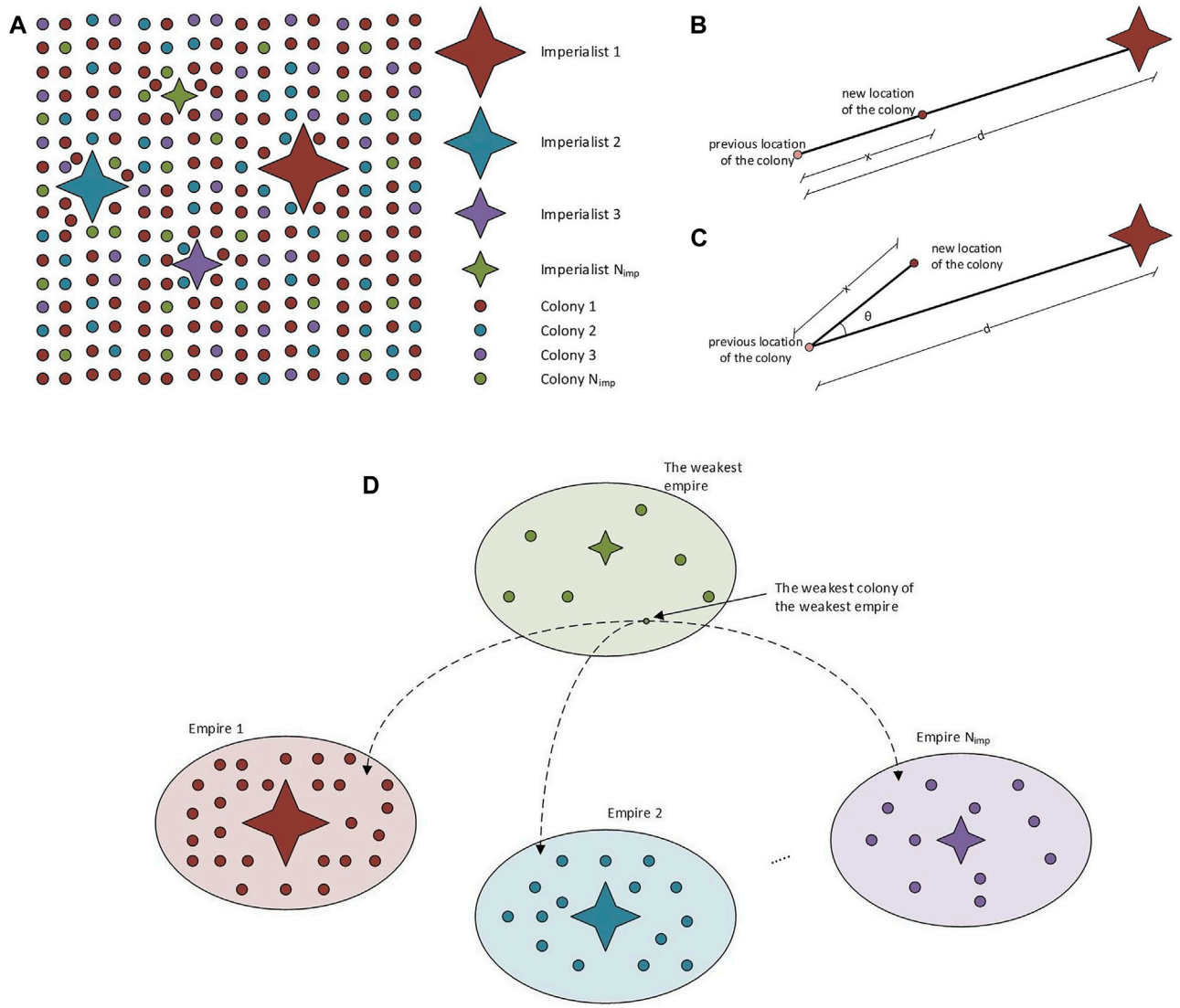

FIGURE 2 | The imperial competitive algorithm. **(A)** Formation of the initial empires. **(B)** Movement of colonies toward their associated colonialist. **(C)** Moving colonies to their associated colonialist with a possible deviant address. **(D)** Imperialist competition. The stronger an empire, the more likely it is to take possession of the weakest colony of the weakest empire.

initial population of size N_{pop} is formed (in the framework of this study and the applications of the IMSFARE project, an initial population of 200 countries was used). The cost of each country is calculated by means of the objective function F of the problem in the variables $(p_1, p_2, \cdots p_n)$. Thus, $cost = F(countr\,y) = F([p_1, p_2, \cdots p_N])$.

Depending on the initial cost of the countries, they are divided into N_{imp} (for the needs of this study and the IMSFARE project N_{imp} was considered equal to 8) where the most powerful ones define the first imperialists and the remaining countries N_{col} represent the initial colonies $(N_{imp} + N_{col} = N_{pop})$. Depending on the cost of the imperialists, the colonies are divided among the imperialists in order to form the initial empires. For this purpose, the normalized cost of each imperialist is defined as $C_n = c_n - max\{c_1, c_2, \cdots c_{N_{imp}}\}$, where c_n is the cost of nth imperialist and C_n is its normalized cost value. Based on the normalized cost value, the power, p_n, of each colonialist can be calculated as follows:

$$p_n = \left| \frac{C_n}{\sum_{i=1}^{N_{imp}} C_i} \right|. \tag{15}$$

Thus, the original colonies pass into the possession of each colonialist and form the first empires, depending on the power of each colonialist according to the relation $NC_n = round(p_n \cdot N_{col})$, which denotes the initial number of colonies in the nth empire. NC_n are randomly selected and assigned to the nth empire. **Figure 2A** shows the initial population of each empire. The strongest empires own the largest number of colonies while the weakest ones possess the smallest.

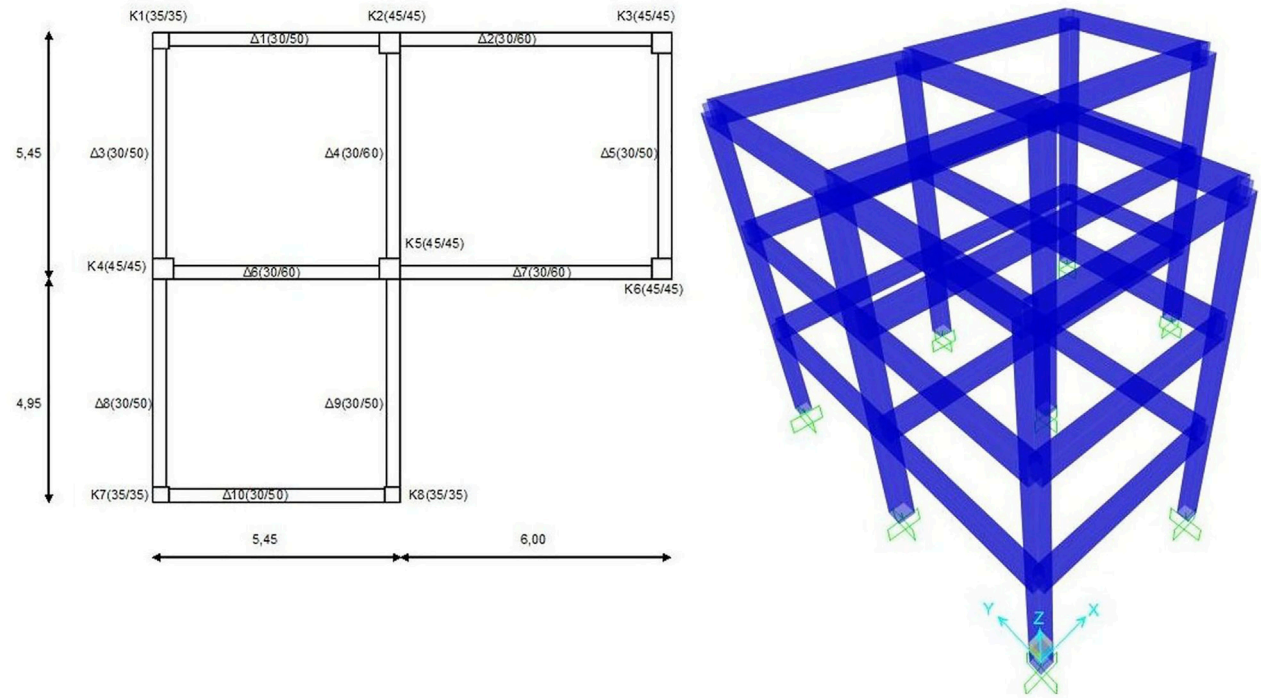

FIGURE 3 | Typical floor plan of the case study building structure and its simulation.

Step 2 (movement of colonies of an empire to the imperialist): once the colonies are divided into empires, they start moving toward their imperialist. In this way, the imperialists improve their colonies by moving the whole population of countries toward positions of lower cost. This movement takes place along the vector joining the colony to the imperialist, as shown in **Figure 2B**. The colony travels a distance of x units in the direction of this vector, which is considered a random variable with uniform distribution $x \approx U(0, \beta \cdot d)$, where β is a number greater than 1 and d is the Euclidean distance between a colony and its imperialist. In most applications, the value $\beta = 2$ gives rapid convergence of countries to the global best. Aiming to enable the search process for the colony in different places around its imperialist, a random deviation in the direction of the movement is provided. This is implemented with the random deviation angle θ (**Figure 2C**), which is a random number with a uniform distribution $\theta \approx U(-\gamma, \gamma)$. In most applications, the value $\gamma = \pi/4$ gives rapid convergence of countries to the global best.

Step 3 (change of position between the colonialist and a colony): if a colony moving toward the colonialist identifies a better position of lower cost than the colonialist, then they change their positions. In other words, this colony becomes the new colonialist of the empire. The algorithm continues with the new colonialist, and the colonies of the empire (including the former colonialist) move toward the new colonialist.

Step 4 (total power of the empire): The total cost of the nth empire is calculated as follows:

$$c_{n,total} = c_n + \xi \cdot average\left(F\left(country_i\right)\right), i = 1, 2, \cdots, NC_n, \quad (16)$$

where the value $\xi = 0.1$ is used in most applications.

Step 5 (imperialist competition): imperialist rivalry gradually leads to loss of power for the weakest empires and strengthening the strongest ones, while all empires try to take possession of colonies of other empires. This is modeled in the algorithm by selecting some of the weakest colonies of the weakest empires and making competition between the other empires over who will acquire these colonies (**Figure 2D**). The empires with the greatest power are most likely to dominate this competition. The normalized cost of the empire is given by $C_{n,total} = c_{n,total} - max\{c_{1,total}, c_{2,total}, \cdots c_{N_{imp},total}\}$, and its power

$$p_{pn} = \left| \frac{C_{n,total}}{\sum_{i=1}^{Nimp} C_{i,total}} \right|. \quad (17)$$

Vector D is defined as $D = P - R = [d_1, d_2, \cdots, d_{N_{imp}}] = [p_{p1} - r_1, p_{p2} - r_2, \cdots, p_{pN_{imp}} - r_{N_{imp}}]$, where P represents the power vector of the empires and R is a vector with random numbers uniformly distributed in the space (0, 1). With reference to vector D, the referenced colonies will be brought to the empire whose element in vector D is the maximum.

Step 6 (exclusion of powerless empires): empires left without colonies are considered collapsing and excluded from the competition.

Step 7 (convergence): in the end, only one empire will remain (the most powerful) after the collapse of the rest, and all colonies

TABLE 1 | Calculation of moment-chord rotation angles θ_y, θ_{um}, and $\theta_{u,pl}$, for the structural elements.

Element	b/h (cm)	d_b (m)	L_{net} (m)	L_s (m)	$(1/R)_y$	$(1/R)_u$	M_y(kNm)	M_u(kNm)	θ_y	θ_{um}	$\theta_{u,pl}$
Beams											
Δ1	30/50	0.016	4.63	2.31	0.0057	0.0579	176.38	194.37	0.0078	0.0566	0.0488
Δ2	30/60	0.020	5.60	2.80	0.0045	0.0579	206.17	242.40	0.0076	0.0568	0.0493
Δ3	30/50	0.016	4.65	2.33	0.0057	0.0579	176.38	194.37	0.0078	0.0568	0.0489
Δ4	30/60	0.020	4.60	2.30	0.0045	0.0579	206.17	242.40	0.0069	0.0530	0.0461
Δ5	30/50	0.016	4.60	2.30	0.0057	0.0579	176.38	194.37	0.0078	0.0565	0.0487
Δ6	30/60	0.020	4.63	2.31	0.0045	0.0579	206.17	242.40	0.0069	0.0531	0.0462
Δ7	30/60	0.020	5.60	2.80	0.0045	0.0579	206.17	242.40	0.0076	0.0568	0.0493
Δ8	30/50	0.016	4.65	2.33	0.0057	0.0579	176.38	194.37	0.0078	0.0568	0.0489
Δ9	30/50	0.016	4.63	2.31	0.0057	0.0579	176.38	194.37	0.0078	0.0566	0.0488
Δ10	30/50	0.016	4.65	2.33	0.0057	0.0579	176.38	194.37	0.0078	0.0568	0.0489
Columns											
K11	35/35	0.02	3.00	1.5	−258.15	0.0091	0.0526	98.37	124.69	0.0090	0.0610
K12	45/45	0.02	3.00	1.5	−698.90	0.0066	0.0439	187.81	253.48	0.0073	0.0595
K13	45/45	0.02	3.00	1.5	−364.74	0.0066	0.0439	187.81	253.48	0.0073	0.0550
K14	45/45	0.02	3.00	1.5	−605.59	0.0066	0.0439	187.81	253.48	0.0073	0.0582
K15	45/45	0.02	3.00	1.5	−1,012.96	0.0066	0.0439	187.81	253.48	0.0073	0.0640
K16	45/45	0.02	3.00	1.5	−327.93	0.0066	0.0439	187.81	253.48	0.0073	0.0546
K17	35/35	0.02	3.00	1.5	−276.97	0.0091	0.0526	98.37	124.69	0.0090	0.0614
K18	35/35	0.02	3.00	1.5	−265.58	0.0091	0.0526	98.37	124.69	0.0090	0.0612
K21	35/35	0.02	3.00	1.5	−172.53	0.0091	0.0526	98.37	124.69	0.0090	0.0590
K22	45/45	0.02	3.00	1.5	−465.53	0.0066	0.0439	187.81	253.48	0.0073	0.0564
K23	45/45	0.02	3.00	1.5	−243.19	0.0066	0.0439	187.81	253.48	0.0073	0.0535
K24	45/45	0.02	3.00	1.5	−403.56	0.0066	0.0439	187.81	253.48	0.0073	0.0556
K25	45/45	0.02	3.00	1.5	−675.45	0.0066	0.0439	187.81	253.48	0.0073	0.0592
K26	45/45	0.02	3.00	1.5	−218.41	0.0066	0.0439	187.81	253.48	0.0073	0.0532
K27	35/35	0.02	3.00	1.5	−184.53	0.0091	0.0526	98.37	124.69	0.0090	0.0593
K28	35/35	0.02	3.00	1.5	−177.96	0.0091	0.0526	98.37	124.69	0.0090	0.0591
K31	35/35	0.02	3.00	1.5	−83.29	0.0091	0.0526	98.37	124.69	0.0090	0.0570
K32	45/45	0.02	3.00	1.5	−233.54	0.0066	0.0439	187.81	253.48	0.0073	0.0534
K33	45/45	0.02	3.00	1.5	−120.23	0.0066	0.0439	187.81	253.48	0.0073	0.0520
K34	45/45	0.02	3.00	1.5	−201.29	0.0066	0.0439	187.81	253.48	0.0073	0.0530
K35	45/45	0.02	3.00	1.5	−347.56	0.0066	0.0439	187.81	253.48	0.0073	0.0548
K36	45/45	0.02	3.00	1.5	−106.91	0.0066	0.0439	187.81	253.48	0.0073	0.0518
K37	35/35	0.02	3.00	1.5	−90.86	0.0091	0.0526	98.37	124.69	0.0090	0.0572
K38	35/35	0.02	3.00	1.5	−86.50	0.0091	0.0526	98.37	124.69	0.0090	0.0571

will be under its occupation. At this point, all colonies are in the same place and have the same cost to each other as to the colonial. In this ideal world, there is no difference between colonies and the colonialist.

5 NUMERICAL TESTS

This section provides the numerical tests for describing the implementation of the proposed design framework to achieve the optimized strengthening of the vertical structural elements of an RC building structure. Aiming to assess and then minimize the torsional response, a three-story RC building structure is considered. The plan view, common for all stories, is gamma-shaped (**Figure 3**) with an area of 89 m^2, and the storys' height is equal to 3 m. It corresponds to a residential building and is located in the Municipality of Zografou (hazard zone Z1, according to the Greek hazard map for the city of Athens (Papazachos et al., 1993).

The building is analyzed as a space frame structural system, where the contribution of infill walls on the structural response against the horizontal loads of the random action (e.g., explosion and earthquake) is neglected. Therefore, it is assumed that these loads are received from the other structural elements, namely, beams, columns, and shear walls, the first two of which are simulated with frame elements having 6-DOF. The slabs are not inserted in the model, but the diaphragm function of the floors is ensured by coupling the story's model nodes, while the ground supports are considered to be fully fixed.

Some characteristics of the construction materials were used. Concrete: the original structural system was considered to use concrete of quality C20/25 with a modulus of elasticity E_{cm} = 29 Gpa. Given that the case study refers to an existing structure that will be assessed by means of inelastic analyses, the average strength is considered, $f_c = \frac{f_{ck}+8}{\gamma_m} = \frac{(20+8)}{1.10} = 25.454\,MPa$. Steel: regarding reinforcing steel quality, S400 was considered, with a modulus of elasticity of Es = 200 Gpa. It was also considered post-yield hardening of 1.10; that is, the failure stress is equal to

Capacity curve, uniform X+03Y		
Step	D (m)	V (KN)
3	-0.0494	1121.98
4	**-0.0711**	**1218.44**
PP	**-0.0810**	**1242.32**
5	**-0.0887**	**1261.43**
6	-0.1206	1311.10

Capacity curve, uniform -X-03Y		
Step	D (m)	V (KN)
4	0.0534	1147.39
5	**0.0747**	**1228.96**
PP	**0.0800**	**1241.47**
6	**0.0876**	**1262.43**
7	0.1082	1294.30

Capacity curve, uniform Y+0.3X		
Step	D (m)	V (KN)
5	-0.0127	1126.46
6	**-0.0159**	**1222.84**
PP	**-0.0170**	**1245.32**
7	**-0.0185**	**1277.45**
8	-0.0220	1323.28

Capacity curve, uniform -Y-0.3X		
Step	D (m)	V (KN)
5	0.0121	1098.54
6	**0.0156**	**1209.40**
PP	**0.0170**	**1241.52**
7	**0.0190**	**1283.93**
8	0.0221	1325.93

Capacity curve, eigenmode based X-0.3Y		
Step	D (m)	V (KN)
4	-0.0603	1029.09
5	**-0.0822**	**1088.46**
PP	**-0.0930**	**1105.41**
6	**-0.1134**	**1138.67**
7	-0.1334	1168.37

Capacity curve, eigenmode based -X+0.3Y		
Step	D (m)	V (KN)
4	0.0482	967.23
5	**0.0715**	**1065.27**
PP	**0.093**	**1106.05**
6	**0.1012**	**1121.53**
7	0.1283	1159.93

Capacity curve, eigenmode based Y-0.3X		
Step	D (m)	V (KN)
5	0.0101	988.06
6	**0.0122**	**1046.97**
PP	**0.013**	**1065.75**
7	**0.0144**	**1096.85**
8	0.0182	1156.52

Capacity curve, eigenmode based -Y+0.3X		
Step	D (m)	V (KN)
5	-0.0085	930.48
6	**-0.0111**	**1019.58**
PP	**-0.013**	**1065.47**
7	**-0.0140**	**1087.01**
8	-0.0174	1140.84

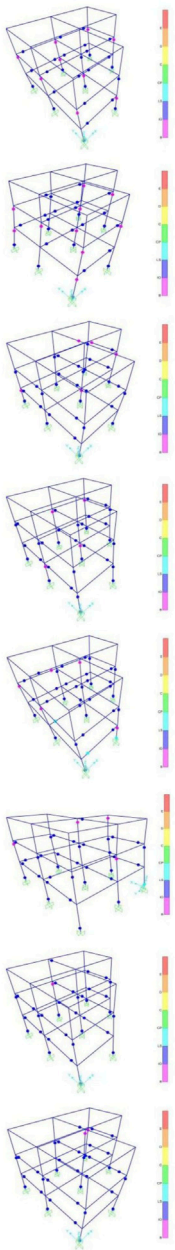

FIGURE 4 | Deformation view of the structural system at the performance point for the different distributions of the horizontal loads.

$f_{tk} = 440\,MP$ and the yield stress is calculated as follows: $f_{sy} = \frac{f_{yk}}{\gamma_m} = \frac{400}{1.10} = 363.636\,MPa$. Beams and columns were grouped according to their dimensions and reinforcement. The longitudinal reinforcement of the original design was 8Ø20 for beams labelled as Δ2, Δ4, Δ6, and Δ7; 10Ø16 for beams Δ1, Δ3, Δ5, Δ8, Δ9, and Δ10; 8Ø20 for columns K1, K7, and K8; and 12Ø20 for columns K2, K3, K4, K5, and K6. The active stiffness of the structural elements is less than the geometric one due to cracking. The reduction of the stiffness was implemented according to the regulation (Earthquake Planning and Protection Organization, 2017). In order to consider the stiffness reduction in analysis/design software, the $\frac{K_{eff}}{K_{el}}$ coefficient is introduced on the modifiers of each section at the moment of inertia.

The vertical loads considered for assessing the building comply with Eurocode 1 (1995). Permanent loading: self-weight of slabs (considering the thickness of 18 cm) is equal to 4.5 kN/m^2, roof covering 1.5 kN/m^2, and infill walls 1.7 kN/m. Live loading: rooms 2.0 kN/m^2. The elastic design spectrum used to evaluate the building in implementing the ATC-40 (Applied Technology Council, 1996) methodology was defined based on EC8. In the specific building, the parameters are Z1 ($a_{gR} = 0.16$), significance II ($\gamma_I = 1.00$), and ground B ($T_B = 0.15$, $T_C = 0.50$, $T_D = 2.50$, $S = 1.20$). Initially, a maximum number of 12 eigenmodes is selected. As already mentioned, the vibrating mass is set for the combination of G + 0.3Q.

It is observed that the first eigenmode is the fundamental one for the Y direction with a mass participation rate of around 83%, while the second eigenmode is the fundamental one for the X direction with a participation rate of around 81%. The primary step in introducing the non-linearity of the members is to define the non-linear properties of the materials. For concrete failure, deformation in compression and bending was considered equal to 2‰ and 3.5‰, respectively, while for steel, the failure deformation was considered equal to 20‰. The ETABS for the extraction of the baring capacity curve during the static inelastic analysis is based on the step-by-step method, that is, the formation of concentrated plastic hinges on the elements until the establishment of the baring collapse mechanism implementing a force-control approach. The next step is the definition of the location of plastic hinges in the structural elements and the definition of their inelastic behavior, that is, the formation of their behavior curve in terms of the moment-chord rotation angle. Given the values of φ_y and φ_u, the value of chord rotation angle for yield and failure, and θ_y and θ_{um}, respectively, for the structural elements, the required quantities are calculated according to KANEPE (Earthquake Planning and Protection Organization, 2017). Note here that $\rho_s = \rho_d = 0$ was considered.

For the calculations in the case of columns, it is necessary to determine the axial forces for the load combination G + 0.3Q (**Table 1**) for beams and columns. In **Table 1**, the first index for the column elements denotes the story and the second one its location in the plan view; that is, K34 is K4 (as denoted in **Figure 4**) at the third story. In **Table 1**, b and h refer to the dimensions of the rectangular cross section; d_b denotes the mean diameter of the longitudinal steel reinforcement; L_{net} and L_s denote the net length of the element and the distance of extreme cross section from the location of zero bending moment, respectively; $(1/R)_y$ and $(1/R)_u$ represent the yield and ultimate capacity values of the curvature; and M_y and M_u symbolize the yield and ultimate bending capacity of the element. A plastic failure mode is selected, and then, depending on the element for which the plastic hinge is defined, the critical failure mode is selected (bending based for the beams and interaction of bending and axial one for the columns). The performance levels of the element are also defined on the curve. Note here that all elements were considered primary, and the positions of the plastic hinge formation are defined at the ends of the beams and columns.

TABLE 2 | Status of plastic hinge in the various steps of pushover analysis.

Step	D (m)	V (kN)	AtoB	BtoIO	IOtoLS	LStoCP	CPtoC	CtoD	DtoE	>E	Total
Uniform X + 03Y											
3	−0.0494	1,121.98	89	2	17	0	0	0	0	0	108
4	−0.0711	1,218.44	81	4	23	0	0	0	0	0	108
5	−0.0887	1,261.43	72	9	27	0	0	0	0	0	108
6	−0.1206	1,311.10	71	3	23	11	0	0	0	0	108
Uniform −X−03Y											
4	0.0534	1,147.39	87	1	20	0	0	0	0	0	108
5	0.0747	1,228.96	79	6	23	0	0	0	0	0	108
6	0.0876	1,262.43	73	10	25	0	0	0	0	0	108
7	0.1082	1,294.30	70	5	25	8	0	0	0	0	108
Uniform Y + 0.3X											
5	−0.0127	1,126.46	90	2	16	0	0	0	0	0	108
6	−0.0159	1,222.84	80	4	24	0	0	0	0	0	108
7	−0.0185	1,277.45	72	5	31	0	0	0	0	0	108
8	−0.0220	1,323.28	70	4	27	7	0	0	0	0	108
Uniform −Y−0.3X											
5	0.0121	1,098.54	93	1	14	0	0	0	0	0	108
6	0.0156	1,209.40	81	1	26	0	0	0	0	0	108
7	0.0190	1,283.93	72	4	32	0	0	0	0	0	108
8	0.0221	1,325.93	70	4	29	5	0	0	0	0	108
Eigenmode-based X−0.3Y											
4	−0.0603	1,029.09	83	5	20	0	0	0	0	0	108
5	−0.0822	1,088.46	74	6	28	0	0	0	0	0	108
6	−0.1134	1,138.67	67	5	33	3	0	0	0	0	108
7	−0.1334	1,168.37	66	3	28	11	0	0	0	0	108
Eigenmode-based −X + 0.3Y											
4	0.0482	967.23	89	7	12	0	0	0	0	0	108
5	0.0715	1,065.27	76	7	25	0	0	0	0	0	108
6	0.1012	1,121.53	69	4	34	1	0	0	0	0	108
7	0.1283	1,159.93	66	3	30	8	0	0	1	0	108
Eigenmode-based Y−0.3X											
5	0.0101	988.06	86	2	20	0	0	0	0	0	108
6	0.0122	1,046.97	78	2	28	0	0	0	0	0	108
7	0.0144	1,096.85	73	1	34	0	0	0	0	0	108
8	0.0182	1,156.52	68	1	32	7	0	0	0	0	108
Eigenmode-based −Y + 0.3X											
5	−0.0085	930.48	93	4	11	0	0	0	0	0	108
6	−0.0111	1,019.58	81	3	24	0	0	0	0	0	108
7	−0.0140	1,087.01	71	2	35	0	0	0	0	0	108
8	−0.0174	1,140.84	68	2	34	4	0	0	0	0	108

5.1 Assessment of the Original RC Building Structural System

5.1.1 Distributions of Horizontal Loads

According to KANEPE, for the needs of the nonlinear static analyses, the application of at least two different load distributions in height is required. Thus, the "uniform" and the "eigenmode-based" distributions are used. The eigenmode-based distribution is in line with the shape of the fundamental eigenmode along the direction examined. As observed through the eigenmode analysis, the fundamental eigenmode along the X direction is the second one, while for the Y direction, it is the first. For spatial superposing of the random actions, the structure according to KANEPE is analyzed for loads in two directions, where the base shear relative contribution 10:3 and 3:10, "positive" and "negative" sign, is also considered and assessment takes place for the most unfavorable stress/strain

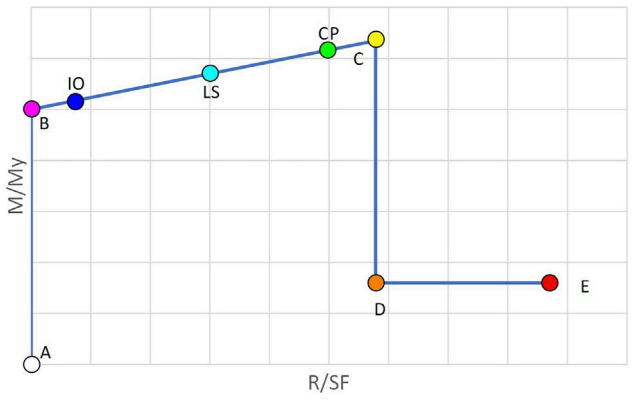

FIGURE 5 | A typical moment rotation curve (M: moment, My: yield moment, R: rotation, SF: safety factor).

quantities observed for each structural element. In particular for both uniform and eigenmode-based distribution + X + 0.3Y and + X−0.3Y (positive direction X); X + 0.3Y and −X−0.3Y (negative direction X), accordingly for Y direction, the application of loads is performed in two phases. Initially, the vertical loads (combination G + 0.3Q) are applied, followed by sixteen nonlinear static analyses for the combination of horizontal loads.

5.1.2 Results of the Assessment

Figure 4 depicts the performance point (PP) along with the previous and next steps of the base shear-deformation (V-D) resistance curve together with the view of the deformed structural system with the location of the formation of the plastic hinges for the eight most unfavorable combinations of horizontal loads. The definition of PP is carried out according to Procedure A described in ATC-40 report [Applied Technology Council (ATC), 1996], and the target displacement is calculated through an iterative procedure using the elastic demand diagram for equivalent damping ratio updated during the iterations. According to Procedure A, the capacity of a structure to resist lateral forces is compared to the demand given by a response spectrum. The response spectrum represents the demand, while the pushover curve (or the "capacity curve") represents the available capacity. The steps of the method are briefly summarized. 1) Perform pushover analysis and determine the capacity curve in base shear (V_b) versus roof displacement of the building (D). This diagram is then converted to acceleration–displacement terms (AD) using an equivalent single degree of system (ESDOF). The conversion is performed using the first mode participation factor C_0 ($D^* = D/C_0$) and the modal mass ($A = V_b/M$). 2) Plot the capacity diagram on the same graph with the 5%-damped elastic response spectrum that is also in AD format. 3) Select a trial peak deformation demand d_t^* and determine the corresponding pseudo-acceleration A from the capacity diagram, initially assuming $\zeta = 5\%$. 4) Compute ductility $\mu = D^*/u_y$ and calculate the hysteretic damping ζ_h as $\zeta_h = 2(\mu - 1)/\pi\mu$. The equivalent damping ratio is evaluated from a relationship of the form $\zeta_{eq} = \zeta_{eq} + \kappa\zeta_h$, where κ is a damping modification factor that depends on the hysteretic behavior of the system. Update the estimate of d_t^* using the elastic demand diagram for ζ_{eq}. 5) Check for convergence of the displacement d_t^*. When convergence has been achieved, the target displacement of the MDOF system is equal to $d_t = C_0 d_t^*$.

In particular, for the uniform distribution by + X (the most unfavorable combination is X + 0.3Y), the analysis based on the uniform X + 0.3Y distribution of the horizontal loading was performed in seven steps. The performance point (V, D) = (1,242.32, −0.0810) was observed between steps 4 and 5. In **Table 2**, it is observed that plastic hinges have been formed in 9 + 27 = 36 edges of structural elements (denoted in pink (BtoIO) and blue (IOtoLS) columns). However, the limit of the chord rotation angle for the "life safety" performance level (blue) has not been exceeded for any of them. The building is therefore considered safe for this distribution of horizontal loads.

For the uniform distribution by −X (worst combination o −X−0.3Y), the analysis based on the uniform −X−0.3Y distribution of the horizontal loading was performed in eight steps. The performance point (V,D) = (1,241.47, 0.080) was observed between steps 5 and 6. In **Table 2**, it is observed that plastic hinges have been formed in 10 + 25 = 35 edges of structural elements (denoted in pink (BtoIO) and blue (IOtoLS) columns). However, the limit of the chord rotation angle for the "life safety" performance level (blue) has been exceeded for any of them. The building is therefore considered safe for this distribution of horizontal loads. For the uniform distribution by + Y (the most unfavorable combination is Y + 0.3X), the analysis based on the uniform Y + 0.3X distribution of the horizontal loading was performed in eleven steps. The performance point (V, D) = (1,245.32, −0.0170) was observed between steps 6 and 7. In **Table 2**, it is observed that plastic hinges have been formed in 5 + 31 = 36 edges of structural elements (denoted in pink (BtoIO) and blue (IOtoLS) columns). However, the limit of the chord rotation angle for the "life safety" performance level (blue) has been exceeded for any of them. The building is therefore considered safe for this distribution of horizontal loads. For the uniform distribution by −Y (worst combination −Y−0.3X), the analysis based on the uniform −Y−0.3X distribution of the horizontal loading was performed in eleven steps. The performance point (V, D) = (1,241.52, 0.017) was observed between steps 6 and 7. In **Table 2**, it is observed that plastic hinges have been formed in 4 + 32 = 36 edges of structural elements (denoted in pink (BtoIO) and blue (IOtoLS) columns). However, the limit of the chord rotation angle for the "life safety" performance level (blue) has been exceeded for any of them. The building is therefore considered safe for this distribution of horizontal loads.

Accordingly, for the eigenmode-based distribution by + X (the most unfavorable combination is X−0.3Y), the analysis based on the eigenmode-based X−0.3Y distribution of the horizontal loading was performed in eight steps. The performance point (V, D) = (1,105.41, −0.093) was observed between steps 5 and 6. In **Table 2**, it is observed that plastic hinges have been formed in 5 + 33 + 3 = 41 edges of structural elements [denoted in pink (BtoIO), blue (IOtoLS), and light blue (LStoCP) columns)]. In three of them, the limit of the chord rotation angle was exceeded for the "life safety" performance level (blue). These elements

TABLE 3 | Status of plastic hinges in the various steps of pushover analysis.

Step	D (m)	V (kN)	AtoB	BtoIO	IOtoLS	LStoCP	CPtoC	CtoD	DtoE	>E	Total
Uniform X + 03Y											
PP init	−0.0810	1,242.32	—	—	—	—	—	—	—	—	—
5	−0.0887	1,261.43	72	9	27	0	0	0	0	0	108
PP streng	−0.0770	1,356.83	—	—	—	—	—	—	—	—	—
5	−0.0772	1,359.61	78	5	25	0	0	0	0	0	108
Uniform −X−03Y											
PP init	0.0800	1,241.47	—	—	—	—	—	—	—	—	—
6	0.0876	1,262.43	73	10	25	0	0	0	0	0	108
PP streng	0.0770	1,347.15	—	—	—	—	—	—	—	—	—
5	0.0935	1,402.22	72	6	30	0	0	0	0	0	108
Uniform Y + 0.3X											
PP init	−0.0170	1,245.32	—	—	—	—	—	—	—	—	—
7	−0.0185	1,277.45	72	5	31	0	0	0	0	0	108
PP streng	−0.0170	1,369.07	—	—	—	—	—	—	—	—	—
4	−0.0194	1,439.69	68	6	34	0	0	0	0	0	108
Uniform −Y−0.3X											
PP init	0.0170	1,241.52	—	—	—	—	—	—	—	—	—
7	0.0190	1,283.93	72	4	32	0	0	0	0	0	108
PP streng	0.0170	1,354.49	—	—	—	—	—	—	—	—	—
6	0.0177	1,373.64	77	2	29	0	0	0	0	0	108
Eigenmode-based X−0.3Y											
PP init	−0.0930	1,105.41	—	—	—	—	—	—	—	—	—
6	−0.1134	1,138.67	67	5	33	3	0	0	0	0	108
PP streng	−0.0880	1,195.85	—	—	—	—	—	—	—	—	—
6	−0.1026	1,224.96	65	7	36	0	0	0	0	0	108
Eigenmode-based −X + 0.3Y											
PP init	0.0930	1,106.05	—	—	—	—	—	—	—	—	—
6	0.1012	1,121.53	69	4	34	1	0	0	0	0	108
PP streng	0.0890	1,200.39	—	—	—	—	—	—	—	—	—
6	0.0924	1,208.42	68	7	33	0	0	0	0	0	108
Eigenmode-based Y−0.3X											
PP init	0.0130	1,065.75	—	—	—	—	—	—	—	—	—
7	0.0144	1,096.85	73	1	34	0	0	0	0	0	108
PP streng	0.0130	1,136.45	—	—	—	—	—	—	—	—	—
6	0.0135	1,141.22	76	2	30	0	0	0	0	0	108
Eigenmode-based −Y + 0.3X											
PP init	-−0.0130	1,065.47	—	—	—	—	—	—	—	—	—
7	−0.0140	1,087.01	71	2	35	0	0	0	0	0	108
PP streng	−0.0130	1,141.32	—	—	—	—	—	—	—	—	—
6	−0.0134	1,142.45	73	4	31	0	0	0	0	0	108

correspond to beams Δ4 and Δ10 of the ground floor and column K18. For the eigenmode-based distribution by −X (most unfavorable combination o −X + 0.3Y), the analysis based on the eigenmode-based −X + 0.3Y distribution of the horizontal loading was performed in seven steps. The performance point (V, D) = (1,106.05, 0.093) was observed between steps 5 and 6. In **Table 2**, it is observed that plastic hinges have been formed in 4 + 34 + 1 = 39 edges of structural elements [denoted in pink (BtoIO), blue (IOtoLS), and light blue (LStoCP) columns)]. In one of them, the limit of the chord rotation angle was exceeded for the "life safety" performance level (blue). This element corresponds to column K17. For the eigenmode-based distribution by + Y (the worst combination is Y−0.3X), the analysis based on the eigenmode-based Y−0.3X distribution of the horizontal loading was performed in ten steps. The performance point (V, D) = (1,065.75, 0.013) was observed between steps 6 and

TABLE 4 | Ground floor data register.

Elem	b (m)	h (m)	ρ	x (m)	y (m)	cc	t_o (m)	ρ_o	E_s(kPa)	E_{cm}(kPa)	l (m)	Ng (kN)	N1 (kN)	N2 (kN)
K1	0.35	0.35	0.0205	0.175	10.225	0.6	0	0	29.10^6	$30.5{\cdot}10^6$	3	239.01	159.10	76.6
K2	0.45	0.45	0.0186	5.225	10.175	0.6	0	0	29.10^6	$30.5{\cdot}10^6$	3	723.36	482.33	242.33
K3	0.45	0.45	0.0186	11.225	10.175	0.6	0	0	29.10^6	$30.5{\cdot}10^6$	3	365.24	243.71	120.41
K4	0.45	0.45	0.0186	0.225	5.175	0.6	0	0	29.10^6	$30.5{\cdot}10^6$	3	620.43	413.29	206.32
K5	0.45	0.45	0.0186	5.225	5.175	0.6	0	0	29.10^6	$30.5{\cdot}10^6$	3	995.15	663.24	340.53
K6	0.45	0.45	0.0186	11.225	5.175	0.6	0	0	29.10^6	$30.5{\cdot}10^6$	3	333.69	221.20	108.23
K7	0.35	0.35	0.0205	0.175	0.175	0.6	0.1	0.014	29.10^6	$30.5{\cdot}10^6$	3	321.73	214.91	107.3
K8	0.35	0.35	0.0205	5.275	0.175	0.6	0	0	29.10^6	$30.5{\cdot}10^6$	3	248.54	165.75	79.95

7. In **Table 2**, it is observed that plastic hinges have been formed in 1 + 34 = 35 edges of structural elements [denoted in pink (BtoIO) and blue (IOtoLS) columns]. However, none of them has exceeded the limit of the chord rotation angle for the "life safety" performance level (blue). The building is therefore considered safe for this distribution of horizontal loads. For the eigenmode-based distribution by −Y (worst combination o −Y + 0.3X), the analysis based on the eigenmode-based −Y + 0.3X distribution of the horizontal loading was performed in ten steps. The performance point (V, D) = (1,065.47, −0.013) was observed between steps 6 and 7. In **Table 2**, it is observed that plastic hinges have been formed in 2 + 35 = 37 edges of structural elements [denoted in pink (BtoIO) and blue (IOtoLS) columns]. However, none of them has exceeded the limit of the chord rotation angle for the "life safety" performance level (blue). The building is therefore considered safe for this distribution of horizontal loads. A typical moment rotation curve along with the notation of the PP and the coloring of **Table 2** and those that follow is provided in **Figure 5**.

Based on the most unfavorable responses of the structural system obtained for the random design action of EC8 (European Committee for standardization ENV 1998-1-1:1994) through the various distributions of horizontal loads, it is concluded that the structural system as a whole is not safe for the specific intensity of the random action because structural elements Δ6 and Δ10 of the ground floor, K17 and K18, develop deformations larger than the acceptable ones, those defined by the "life safety" performance level in terms of the chord rotation angle. The next step is to strengthen some of these elements to enter the safe region.

5.2 Strengthening Based on Design Provisions

Based on the investigation of the previous section during the assessment of the structural system presented, for some elements (Δ6 and Δ10 of the ground floor, K17, K18), the chord rotation angle exceeded the limit set for "life safety" performance level defined by Kanepe (2017); that is, these elements during the design earthquake develop damage greater than acceptable. Given that all the structural elements are considered primary, the specific structural system as a whole is not considered safe. For this reason, in this part of the investigation, strengthening interventions of these elements will be examined so that the redesigned structural system meets the design goal B1 of Kanepe (2017), that is, for the design earthquake (10% probability of exceeding within the conventional life time of 50 years), all structural elements of the construction to be located before the level corresponding to the "life safety" performance level. After various tests of interventions that did not always have positive results for the redesigned structural system, strengthening column K7 along its height with RC jacketing was selected. The process of strengthening and re-assessment of the redesigned structural system, during which this new design is considered safe (meeting the design objective), is described in this section.

A 10 cm RC jacketing with 8Ø20 reinforcement is used to strengthen column K7. The strengthened structural system is assessed by means of nonlinear static analyses based on the distributions of the horizontal loads. Note that for the strengthened structural system, the first eigenmode is the fundamental one along the Y direction while the second one is along the X direction. In **Table 3**, the performance points for the strengthened structural system are compared with those of the original one.

As observed from **Table 3**, the performance points of the strengthened structural system for the various loading combinations show a small increase of the base shear by 90–130 kN, of the order of about 8%. As far as the target displacements are concerned, they are significantly reduced for the distributions of the X direction while they practically remain unchanged for the distributions of the Y direction. This can be partially explained as follows: in the X direction, column K7 participates in the baring frame K7-Δ10-K8, where both columns K7 and K8 contribute with the less rigid orientation of their cross section. Thus, it becomes the weakest one among all baring frames of the structural system. Along the Y direction, strengthening did not contribute significantly because the Y-baring frames were originally more rigid. Due to the reduction of target displacements along the X direction, no structural element of the redesigned structural system develops any longer damage for the design earthquake larger than the acceptable ones, those defined by the "life safety" performance level. For the original structural system, distributions along the X direction developed structural elements exceeding this performance level. In addition, the number of edges entering the plastic zone was also reduced in most loading distributions. As a general conclusion, it can be said that the specific strengthening operation is considered successful because the redesigned structural system is now safe and shows better structural behavior for the design earthquake.

TABLE 5 | Stiffness and strength eccentricities for the two structural systems.

	Stiffness eccentricity		Strength eccentricity					
	Same for all stories		Ground story		1st story		2nd story	
	Original	Strengthened	Original	Strengthened	Original	Strengthened	Original	Strengthened
x_{CR} (m)	5.77	4.67	5.29	4.75	5.33	4.73	5.40	4.72
y_{CR} (m)	6.52	5.27	6.33	5.68	6.33	5.61	6.33	5.52
$e_{CM\text{-}CR}$ or $e_{CM\text{-}CV}$ (m)	1.03	0.86	0.52	0.44	0.55	0.50	0.63	0.60
Variation (%)	−17%		−15%		−9%		−5%	

TABLE 6 | Column reinforcement thickness to minimize the strength eccentricity of the second floor.

Column	2nd story (Problem A)		1st story (Problem B)		Ground story (Problem C)	
	RC jacket		RC jacket		RC jacket	
	Thickness (cm)	Reinforcement percentage	Thickness (cm)	Reinforcement percentage	Thickness (cm)	Reinforcement percentage
K1	20	0.0260	0	0.0	20	0.0290
K2	20	0.0167	20	0.0400	0	0
K3	16	0.0278	0	0.0	0	0
K4	0	0.0	16	0.0314	0	0
K5	20	0.0400	0	0.0	20	0.0216
K6	0	0.0	20	0.0100	15	0.0296
K7	10	0.0400	0	0.0	10	0.0100
K8	15	0.0400	20	0.0255	0	0

TABLE 7 | Minimized strength eccentricity values obtained for the tree problems.

Story	$e_{CM\text{-}CV}$ (m)		
	Problem A	Problem B	Problem C
Ground	0.0290	0.0094	0.0003
1st	0.0162	0.0018	0.0143
2nd	0.00063	0.0065	0.0260

5.3 Strengthening Based on Minimizing Torsional Response

In this part of the study, the process described previously for calculating the components of the problem formulations is integrated into the ICA algorithm, aiming to minimize the torsional response of the building. Previously, the structural system was strengthened to meet the design target B1 of Kanepe (2017); then, two cases are considered for strengthening the structural system based on improved torsional response: minimum stiffness and strength eccentricities. As a result, the following information is obtained through the solution of the two optimization problems: 1) thickness of RC jacketing to strengthen the columns, in case of minimizing stiffness eccentricity, and 2) thickness and reinforcement of RC jacketing to strengthen the columns, in case of minimizing the eccentricity of strengths. The designs obtained for the two cases are assessed by means of nonlinear static analyses in comparison with the original design (OD: original design) and the re-design based on strengthening by Kanepe (2017) (KSD: KANEPE based strengthened design). For the implementation of the ICA-based strengthening design framework, a set of data needs to be provided required by the formulation of the optimization problem. Based on these data and with reference to the problem formulation (rigidity or strength eccentricity) during the iterations of the ICA search procedure, new designs, defined with respect to the location, width, and reinforcement of the RC jacketing of each vertical structural element, are derived. For handling the discrete design variables, the procedure described by Lagaros et al. (2022) is followed, according to which they are treated as equivalent continuous variables, using the correction function of the following simple expression:

$$t_j = \frac{floor\left(t_j \times 10\right)}{10}, \; for\; discrete\; variables\; of\; 0.1\; step\; size. \tag{18}$$

5.3.1 Entry of Building Data Into Problem Formulation

According to the previous description, the data required for the two problem formulations are configured (**Table 4**) below.

The plan view is the same for all stories, and the only difference can be found in the last column corresponding to the axial forces of the columns. The axial forces of the columns are obtained by means of linear analyses of KBD for the combination G + 0.3Q. Regarding the minimization problem of strength eccentricity, three cases will be examined (one for each story). The solution corresponding to the best compromise solution will be adopted, where lower eccentricities for all three stories are derived. The data required (columns 2 to 13 of **Table 4**) for solving the minimization

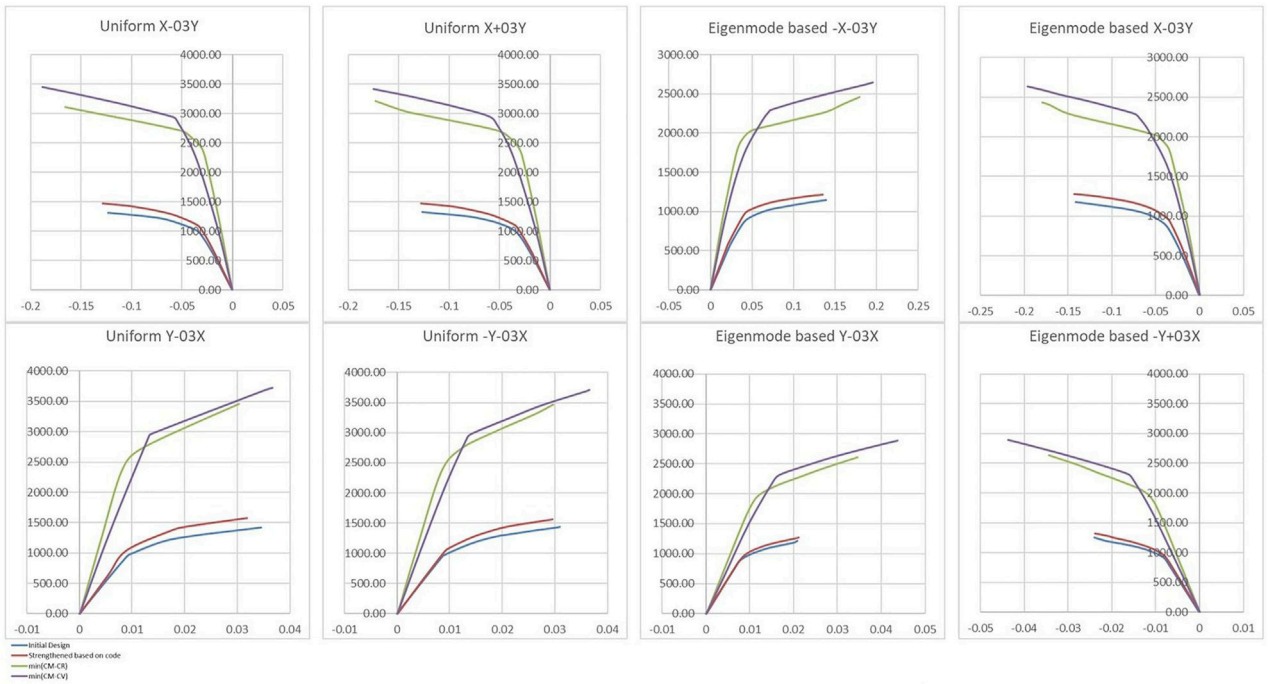

FIGURE 6 | Capacity curves.

problem of stiffness eccentricity are the same for all three stories. In particular, for each vertical structural element, ρ and ρ_o denote the percentage of longitudinal reinforcement and the one of existing RC jackets, respectively; t_o refers to the width of the RC jackets; x and y denote the coordinates of the center of mass; and cc is the cracking coefficient; that is, *Ng* stands for the axial force of the ground floor, *N1* of the first floor, and *N2* for the second one. For the RC jacketing, concrete quality C20/25 is considered, as well as steel reinforcement B500C. The mass centers of all floors coincide because the plan view is the same for all stories, thus creating a centripetal axis for the building. Uniform distribution of the vertical loads was considered on the floor slabs; thus, the mass center coincides with the geometric center of the floors.

5.3.2 Eccentricities of Initial and Strengthened by KANEPE Structural System

The eccentricities of the original structural system and those of the strengthened one are calculated first (**Table 5**), where variation stands for the reduction of the eccentricity values corresponding to the strengthened design compared to the ones of the original design. The axial forces used to calculate the strength eccentrics are derived from linear analyses performed for the two structural systems (OD and KBD) for the combination G + 0.3Q. For the case of KBD, they are identical to those of **Table 4**.

5.3.3 Minimize Stiffness Eccentricity

In this part of the study, the problem of the minimum rigidity eccentricity problem is solved and the results obtained are discussed. The specific problem is formulated once. Thus, a unique solution is derived for all three stories. Given that ICA is an evolutionary search algorithm, it operates based on a population of solutions. The convergence history records the best solution found so far and that of the average value among the population members. Although the convergence history of the optimization procedure takes place shortly before the 2000 iterations, ICA managed to significantly reduce the stiffness eccentricity (cost function) value in less than 500 iterations. When an empire is left, the average cost is equal to the minimum. The optimal solution is located in the position (imperialist position) (0.19, 0.20, 0, 0.20, 0.15, 0.20, 0, 0.19) and has a cost, that is, giving value to the objective function of the problem (imperialist cost) equal to e = 0.0074 m ≈ 7 mm. Each column will therefore be reinforced accordingly. The K7 column is already reinforced with a 10 cm RC jacket. Its final RC jacket will be 10 cm. The RC jackets, for the design of the new body with the minimized rigidity eccentricity, are introduced with the minimum mechanical reinforcement rate of 1%.

5.3.4 Minimize Strength Eccentricity

In this part of the study, the minimum strength eccentricity problem is solved and the results obtained are discussed. The iteration histories of the problems solved independently for the three stories are obtained. Similar to the problem of minimum rigidity, the convergence history is recorded for each of the three problems solved, with respect to the best solution found so far and the average objective function value. The strength eccentricity minimization problem is more time-consuming (1 min/iteration) in contrast to the stiffness eccentricity one, where 2,500 iterations

TABLE 8 | Status of plastic hinges in the various steps of pushover analysis.

Step	D (m)	V (kN)	AtoB	BtoIO	IOtoLs	LStoCP	CPtoC	CtoD	DtoE	>E	Total
Uniform X + 03Y											
PP IN	–0.0810	1,242.32	—	—	—	—	—	—	—	—	—
5	–0.0887	1,261.43	72	9	27	0	0	0	0	0	108
PP DC	–0.0770	1,356.83	—	—	—	—	—	—	—	—	—
5	–0.0772	1,359.61	78	5	25	0	0	0	0	0	108
PP CR	–0.0530	2,715.96	—	—	—	—	—	—	—	—	—
6	–0.0707	2,789.60	69	1	38	0	0	0	0	0	108
PP CV	–0.0610	2,947.67	—	—	—	—	—	—	—	—	—
4	–0.0610	2,954.88	73	9	26	0	0	0	0	0	108
Uniform –X–03Y											
PP IN	0.0800	1,241.47	—	—	—	—	—	—	—	—	—
6	0.0876	1,262.43	73	10	25	0	0	0	0	0	108
PP DC	0.0770	1,347.15	—	—	—	—	—	—	—	—	—
5	0.0935	1,402.22	72	6	30	0	0	0	0	0	108
PP CR	0.0540	2,714.78	—	—	—	—	—	—	—	—	—
6	0.0851	2,830.27	68	0	40	0	0	0	0	0	108
PP CV 5	0.0600	2,942.17	—	—	—	—	—	—	—	—	—
5	0.0614	2,960.08	70	11	27	0	0	0	0	0	108
Uniform Y + 0.3X											
PP IN	–0.0170	1,245.32	—	—	—	—	—	—	—	—	—
7	–0.0185	1,277.45	72	5	31	0	0	0	0	0	108
PP DC	-0.0170	1,369.07	—	—	—	—	—	—	—	—	—
4	–0.0194	1,439.69	68	6	34	0	0	0	0	0	108
PP CR	–0.0130	2,762.90	—	—	—	—	—	—	—	—	—
6	–0.0168	2,950.89	68	1	39	0	0	0	0	0	108
PP CV	–0.0140	2,987.62	—	—	—	—	—	—	—	—	—
3	–0.0139	2,984.51	74	7	27	0	0	0	0	0	108
Uniform –Y–0.3X											
PP IN	0.0170	1,241.52	—	—	—	—	—	—	—	—	—
7	0.0190	1,283.93	72	4	32	0	0	0	0	0	108
PP DC	0.0170	1,354.49	—	—	—	—	—	—	—	—	—
6	0.0177	1,373.64	77	2	29	0	0	0	0	0	108
PP CR	0.0130	2,769.07	—	—	—	—	—	—	—	—	—
4	0.0188	3,023.95	68	1	39	0	0	0	0	0	108
PP CV	0.0140	2,966.24	—	—	—	—	—	—	—	—	—
4	0.0141	2,974.64	73	5	30	0	0	0	0	0	108
Eigenmode-based X–0.3Y											
PP IN	–0.0930	1,105.41	—	—	—	—	—	—	—	—	—
6	–0.1134	1,138.67	67	5	33	3	0	0	0	0	108
PP DC	–0.0880	1,195.85	—	—	—	—	—	—	—	—	—
6	–0.1026	1,224.96	65	7	36	0	0	0	0	0	108
PP CR	–0.0640	2063.18	—	—	—	—	—	—	—	—	—
6	–0.0808	2,113.77	70	0	38	0	0	0	0	0	108
PP CV	–0.0690	2,241.80	—	—	—	—	—	—	—	—	—
5	–0.0745	2,289.60	68	9	31	0	0	0	0	0	108
Eigenmode-based –X + 0.3Y											
PP IN	0.0930	1,106.05	—	—	—	—	—	—	—	—	—
6	0.1012	1,121.53	69	4	34	1	0	0	0	0	108
PP DC	0.0890	1,200.39	—	—	—	—	—	—	—	—	—
6	0.0924	1,208.42	68	7	33	0	0	0	0	0	108
PP CR	0.0630	2059.63	—	—	—	—	—	—	—	—	—
6	0.0751	2093.18	68	3	37	0	0	0	0	0	108
PP CV	0.0690	2,240.31	—	—	—	—	—	—	—	—	—
5	0.0747	2,293.44	68	11	29	0	0	0	0	0	108

(Continued on following page)

TABLE 8 | (*Continued*) Status of plastic hinges in the various steps of pushover analysis.

Step	D (m)	V (kN)	AtoB	BtoIO	IOtoLs	LStoCP	CPtoC	CtoD	DtoE	>E	Total
Eigenmode-based Y–0.3X											
PP IN	0.0930	1,106.05	—	—	—	—	—	—	—	—	—
6	0.1012	1,121.53	69	4	34	1	0	0	0	0	108
PP DC	0.0890	1,200.39	—	—	—	—	—	—	—	—	—
6	0.0924	1,208.42	68	7	33	0	0	0	0	0	108
PP CR	0.0630	2059.63	—	—	—	—	—	—	—	—	—
6	0.0751	2093.18	68	3	37	0	0	0	0	0	108
PP CV	0.069	2,240.31	—	—	—	—	—	—	—	—	—
5	0.0747	2,293.44	68	11	29	0	0	0	0	0	108
Eigenmode-based –Y + 0.3X											
PP IN	–0.0130	1,065.47	—	—	—	—	—	—	—	—	—
7	–0.0140	1,087.01	71	2	35	0	0	0	0	0	108
PP DC	–0.0130	1,141.32	—	—	—	—	—	—	—	—	—
6	–0.0134	1,142.45	73	4	31	0	0	0	0	0	108
PP CR	–0.0160	2,138.10	—	—	—	—	—	—	—	—	—
6	–0.0188	2,221.73	67	1	40	0	0	0	0	0	108
PP CV	–0.0160	2,311.81	—	—	—	—	—	—	—	—	—
5	–0.0164	2,317.61	69	8	31	0	0	0	0	0	108

were performed in just a few minutes. Thus, fewer iterations were chosen to identify convergence (around 100). However, as shown in the above history diagrams, the strength eccentricity value is reduced quickly, reaching zero during the first 40 to 80 iterations. Specifically, the optimal solution is located in the position (imperialist position) reported for all three stories in **Table 6**.

The cost values obtained for the three problems A, B, and C along with the eccentricities of the other two stories are provided in **Table 7**. For Problem A, the imperialist cost value is equal to e = 0.00063 m < 1 mm. For Problem B, the imperialist cost value is equal to e = 0.0018 m ≈ 2 mm. For Problem C, the imperialist cost value is equal to e = 0.0003 m < 1 mm. For this solution, the strength eccentricities of the other floors of the building are as follows:

It can be noticed that the optimal floor solutions show a sensitivity because they differ quite a lot from floor to floor. Nevertheless, the optimal solution obtained for the first floor (Problem B) gives low values of eccentricity to the other floors (less than 1 cm). Therefore, it is neither realistic nor practical to use different RC jacketing for a given column along the stories of the building. The strengthening solution obtained through Problem B, according to **Table 7**, is used.

5.4 Assessment of the Strengthened Structural Systems

5.4.1 Eigenmode Analyses

The results of the eigenmode analyses performed for each of the two new structural systems derived through minimization of the eccentricities are presented below. Based on the eigenvalue analyses results, it seems that, for both structural systems, the first eigenmode is the fundamental one along the Y direction while the second eigenmode is the fundamental one along the X direction. It is also worth mentioning that the first three eigenperiod values were significantly reduced in relation to the ones of the original structural system, as expected because due to strengthening, the structural systems became significantly more rigid compared to the original one. Also, note that the mass participation rate of the third eigenmode, which is mainly torsional, was decreased.

5.4.2 Nonlinear Static Analyses

Nonlinear static analyses are performed for the two new structural systems. Their seismic behavior is compared with the corresponding one of the original and the strengthened ones designed to meet the B1 goal of Kanepe (2017). The 16 distributions of the horizontal loads mentioned earlier are also used to perform these analyses. The capacity curves derived are presented first (**Figure 6**), where an estimate of how the interventions affected the overall behavior of the structural systems can be obtained. For every horizontal load distribution, two groups of curves are obtained: those of the original and strengthened designs and those of the designs obtained through eccentricities minimization. These two groups of curves show similar stiffness and capacity. As observed in **Figure 6**, the ultimate load capacity and the initial stiffness of the designs obtained through eccentricity minimization were almost doubled, while the post-cracking stiffness was increased slightly.

Subsequently, the behavior of the structural systems measured for the design earthquake (target displacement, yield base shear demand) for the most unfavorable distributions per direction is presented. Finally, the tables containing the ductility demand of the columns also for the design earthquake are presented. The structural systems derived through the optimization process in comparison to the original and strengthened based on Kanepe (2017) depict a large increase in the stiffness and bearing capacity (almost doubled) and a significant increase in ductility due to the extensive use of RC jackets at the columns. In **Table 8** the following notations are used, performance points for the initial

TABLE 9 | Required ductility values of the columns for the distributions of the horizontal loads.

	Initial design			Strengthened by							
				Code			min (CM-CR)			min (CM-CV)	
	θ_y	$\theta_{pl,dem}$	μ_{dem}	θ_y	$\theta_{pl,dem}$	μ_{dem}	θ_y	$\theta_{pl,dem}$	μ_{dem}	θ_y	$\theta_{pl,dem}$	μ_{dem}
Ground floor columns—uniform distribution X + 0.3Y												
K11up	0.0090	0.0000	1.00	0.0090	0.0000	1.00	0.0081	0.0000	1.00	0.0090	0.0000	1.00
K11dn		0.0096	2.07		0.0072	1.80		0.0041	1.51		0.0000	1.00
K12up	0.0073	0.0000	1.00	0.0073	0.0000	1.00	0.0078	0.0000	1.00	0.0087	0.0000	1.00
K12dn		0.0107	2.47		0.0086	2.18		0.0046	1.59		0.0000	1.00
K13up	0.0073	0.0000	1.00	0.0073	0.0000	1.00	0.0073	0.0000	1.00	0.0073	0.0000	1.00
K13dn		0.0106	2.45		0.0086	2.17		0.0033	1.45		0.0009	1.12
K14up	0.0073	0.0000	1.00	0.0073	0.0000	1.00	0.0078	0.0000	1.00	0.0084	0.0000	1.00
K14dn		0.0094	2.29		0.0069	1.94		0.0045	1.58		0.0004	1.05
K15up	0.0073	0.0004	1.06	0.0073	0.0000	1.00	0.0085	0.0000	1.00	0.0073	0.0000	1.00
K15dn		0.0100	2.37		0.0074	2.01		0.0044	1.51		0.0004	1.06
K16up	0.0073	0.0000	1.00	0.0073	0.0000	1.00	0.0078	0.0000	1.00	0.0077	0.0000	1.00
K16dn		0.0103	2.41		0.0076	2.04		0.0046	1.59		0.0023	1.30
K17up	0.0090	0.0000	1.00	0.0094	0.0000	1.00	0.0098	0.0000	1.00	0.0098	0.0000	1.00
K17dn		0.0085	1.95		0.0072	1.76		0.0031	1.32		0.0009	1.09
K18up	0.0090	0.0003	1.04	0.0090	0.0000	1.00	0.0081	0.0000	1.00	0.0085	0.0000	1.00
K18dn		0.0100	2.11		0.0067	1.75		0.0042	1.52		0.0008	1.09
μ	—	—	1.64	—	—	1.48	—	—	1.26	—	—	1.04
σ	—	—	0.64	—	—	0.49	—	—	0.26	—	—	0.08
CoV	—	—	0.39	—	—	0.33	—	—	0.21	—	—	0.07
1st story columns—uniform distribution X + 0.3Y												
K21up	0.0090	0.0009	1.10	0.0090	0.0000	1.00	0.0081	0.0000	1.00	0.0090	0.0000	1.00
K21dn		0.0000	1.00		0.0000	1.00		0.0000	1.00		0.0000	1.00
K22up	0.0073	0.0024	1.33	0.0073	0.0013	1.18	0.0078	0.0000	1.00	0.0087	0.0000	1.00
K22dn		0.0000	1.00		0.0000	1.00		0.0000	1.00		0.0000	1.00
K23up	0.0073	0.0013	1.17	0.0073	0.0000	1.00	0.0073	0.0000	1.00	0.0073	0.0000	1.00
K23dn		0.0000	1.00		0.0000	1.00		0.0000	1.00		0.0000	1.00
K24up	0.0073	0.0000	1.00	0.0073	0.0000	1.00	0.0078	0.0000	1.00	0.0084	0.0000	1.00
K24dn		0.0000	1.00		0.0000	1.00		0.0000	1.00		0.0000	1.00
K25up	0.0073	0.0028	1.38	0.0073	0.0012	1.17	0.0085	0.0000	1.00	0.0073	0.0000	1.00
K25dn		0.0000	1.00		0.0000	1.00		0.0000	1.00		0.0000	1.00
K26up	0.0073	0.0013	1.18	0.0073	0.0000	1.00	0.0078	0.0000	1.00	0.0077	0.0000	1.00
K26dn		0.0000	1.00		0.0000	1.00		0.0000	1.00		0.0000	1.00
K27up	0.0090	0.0011	1.13	0.0094	0.0000	1.00	0.0098	0.0000	1.00	0.0098	0.0000	1.00
K27dn		0.0000	1.00		0.0000	1.00		0.0000	1.00		0.0000	1.00
K28up	0.0090	0.0026	1.29	0.0090	0.0008	1.09	0.0081	0.0000	1.00	0.0085	0.0000	1.00
K28dn		0.0000	1.00		0.0000	1.00		0.0000	1.00		0.0000	1.00
μ	—	—	1.10	—	—	1.03	—	—	1.00	—	—	1.00
σ	—	—	0.13	—	—	0.06	—	—	0.00	—	—	0.00
CoV	—	—	0.12	—	—	0.06	—	—	0.00	—	—	0.00
2nd story columns—uniform distribution X + 0.3Y												
K31up	0.0090	0.0000	1.00	0.0090	0.0000	1.00	0.0081	0.0000	1.00	0.0090	0.0014	1.16
K31dn		0.0000	1.00		0.0000	1.00		0.0000	1.00		0.0000	1.00
K32up	0.0073	0.0000	1.00	0.0073	0.0000	1.00	0.0078	0.0000	1.00	0.0087	0.0000	1.00
K32dn		0.0000	1.00		0.0000	1.00		0.0000	1.00		0.0000	1.00
K33up	0.0073	0.0000	1.00	0.0073	0.0000	1.00	0.0073	0.0000	1.00	0.0040	0.0000	1.00
K33dn		0.0000	1.00		0.0000	1.00		0.0000	1.00		0.0000	1.00
K34up	0.0073	0.0000	1.00	0.0073	0.0000	1.00	0.0078	0.0000	1.00	0.0084	0.0000	1.00
K34dn		0.0000	1.00		0.0000	1.00		0.0000	1.00		0.0000	1.00
K35up	0.0073	0.0000	1.00	0.0073	0.0000	1.00	0.0085	0.0000	1.00	0.0073	0.0019	1.26
K35dn		0.0000	1.00		0.0000	1.00		0.0000	1.00		0.0000	1.00
K36up	0.0073	0.0000	1.00	0.0073	0.0000	1.00	0.0078	0.0000	1.00	0.0077	0.0000	1.00
K36dn		0.0000	1.00		0.0000	1.00		0.0000	1.00		0.0000	1.00
K37up	0.0090	0.0000	1.00	0.0098	0.0000	1.00	0.0098	0.0000	1.00	0.0098	0.0000	1.00
K37dn		0.0000	1.00		0.0000	1.00		0.0000	1.00		0.0000	1.00
K38up	0.0090	0.0000	1.00	0.0090	0.0000	1.00	0.0081	0.0000	1.00	0.0085	0.0000	1.00
K38dn		0.0000	1.00		0.0000	1.00		0.0000	1.00		0.0000	1.00

(Continued on following page)

TABLE 9 | (*Continued*) Required ductility values of the columns for the distributions of the horizontal loads.

	Initial design			Strengthened by							
				Code			min (CM-CR)			min (CM-CV)	
	θ_y	$\theta_{pl,dem}$	μ_{dem}	θ_y	$\theta_{pl,dem}$	μ_{dem}	θ_y	$\theta_{pl,dem}$	μ_{dem}	θ_y	$\theta_{pl,dem}$	μ_{dem}
μ	—	—	1.00	—	—	1.00	—	—	1.00	—	—	1.03
σ	—	—	0.00	—	—	0.00	—	—	0.00	—	—	0.07
CoV	—	—	0.00	—	—	0.00	—	—	0.00	—	—	0.07
Ground floor columns—uniform distribution Y + 0.3X												
K11up	0.0090	0.0003	1.03	0.0090	0.0000	1.00	0.0081	0.0000	1.00	0.0090	0.0000	1.00
K11dn		0.0028	1.32		0.0022	1.25		0.0016	1.19		0.0000	1.00
K12up	0.0073	0.0000	1.00	0.0073	0.0000	1.00	0.0078	0.0000	1.00	0.0087	0.0000	1.00
K12dn		0.0034	1.46		0.0027	1.37		0.0016	1.21		0.0000	1.00
K13up	0.0073	0.0000	1.00	0.0073	0.0000	1.00	0.0073	0.0000	1.00	0.0073	0.0000	1.00
K13dn		0.0035	1.48		0.0027	1.37		0.0014	1.19		0.0004	1.05
K14up	0.0073	0.0000	1.00	0.0073	0.0000	1.00	0.0078	0.0000	1.00	0.0084	0.0000	1.00
K14dn		0.0030	1.40		0.0030	1.41		0.0016	1.20		0.0001	1.02
K15up	0.0073	0.0000	1.00	0.0073	0.0000	1.00	0.0085	0.0000	1.00	0.0073	0.0000	1.00
K15dn		0.0033	1.45		0.0035	1.48		0.0013	1.16		0.0002	1.03
K16up	0.0073	0.0000	1.00	0.0073	0.0000	1.00	0.0078	0.0000	1.00	0.0077	0.0000	1.00
K16dn		0.0024	1.33		0.0027	1.37		0.0016	1.21		0.0007	1.10
K17up	0.0090	0.0000	1.00	0.0094	0.0000	1.00	0.0098	0.0000	1.00	0.0098	0.0000	1.00
K17dn		0.0033	1.37		0.0035	1.37		0.0014	1.14		0.0003	1.03
K18up	0.0090	0.0000	1.00	0.0090	0.0000	1.00	0.0081	0.0000	1.00	0.0085	0.0000	1.00
K18dn		0.0024	1.26		0.0036	1.40		0.0017	1.21		0.0002	1.03
μ	—	—	1.19	—	—	1.19	—	—	1.09	—	—	1.02
σ	—	—	0.20	—	—	0.19	—	—	0.10	—	—	0.03
CoV	—	—	0.16	—	—	0.16	—	—	0.09	—	—	0.03
1st story columns—uniform distribution Y + 0.3X												
K21up	0.0090	0.0006	1.07	0.0090	0.0004	1.05	0.0081	0.0000	1.00	0.0090	0.0000	1.00
K21dn		0.0000	1.00		0.0000	1.00		0.0000	1.00		0.0000	1.00
K22up	0.0073	0.0006	1.08	0.0073	0.0003	1.04	0.0078	0.0000	1.00	0.0087	0.0000	1.00
K22dn		0.0000	1.00		0.0000	1.00		0.0000	1.00		0.0000	1.00
K23up	0.0073	0.0030	1.41	0.0073	0.0002	1.03	0.0073	0.0000	1.00	0.0073	0.0000	1.00
K23dn		0.0000	1.00		0.0000	1.00		0.0000	1.00		0.0000	1.00
K24up	0.0073	0.0007	1.10	0.0073	0.0005	1.06	0.0078	0.0000	1.00	0.0084	0.0000	1.00
K24dn		0.0000	1.00		0.0000	1.00		0.0000	1.00		0.0000	1.00
K25up	0.0073	0.0006	1.08	0.0073	0.0005	1.07	0.0085	0.0000	1.00	0.0073	0.0000	1.00
K25dn		0.0000	1.00		0.0000	1.00		0.0000	1.00		0.0000	1.00
K26up	0.0073	0.0000	1.00	0.0073	0.0000	1.00	0.0078	0.0000	1.00	0.0077	0.0000	1.00
K26dn		0.0000	1.00		0.0000	1.00		0.0000	1.00		0.0000	1.00
K27up	0.0090	0.0007	1.08	0.0094	0.0000	1.00	0.0098	0.0000	1.00	0.0098	0.0000	1.00
K27dn		0.0000	1.00		0.0000	1.00		0.0000	1.00		0.0000	1.00
K28up	0.0090	0.0005	1.06	0.0090	0.0038	1.42	0.0081	0.0000	1.00	0.0085	0.0000	1.00
K28dn		0.0000	1.00		0.0000	1.00		0.0000	1.00		0.0000	1.00
μ	—	—	1.05	—	—	1.04	—	—	1.00	—	—	1.00
σ	—	—	0.10	—	—	0.10	—	—	0.00	—	—	0.00
CoV	—	—	0.09	—	—	0.10	—	—	0.00	—	—	0.00
2nd story columns—uniform distribution Y + 0.3X												
K31up	0.0090	0.0000	1.00	0.0090	0.0000	1.00	0.0081	0.0000	1.00	0.0090	0.0002	1.03
K31dn		0.0000	1.00		0.0000	1.00		0.0000	1.00		0.0000	1.00
K32up	0.0073	0.0000	1.00	0.0073	0.0000	1.00	0.0078	0.0000	1.00	0.0087	0.0000	1.00
K32dn		0.0000	1.00		0.0000	1.00		0.0000	1.00		0.0000	1.00
K33up	0.0073	0.0000	1.00	0.0073	0.0000	1.00	0.0073	0.0000	1.00	0.0040	0.0000	1.00
K33dn		0.0000	1.00		0.0000	1.00		0.0000	1.00		0.0000	1.00
K34up	0.0073	0.0000	1.00	0.0073	0.0001	1.01	0.0078	0.0000	1.00	0.0084	0.0000	1.00
K34dn		0.0000	1.00		0.0000	1.00		0.0000	1.00		0.0000	1.00
K35up	0.0073	0.0000	1.00	0.0073	0.0001	1.01	0.0085	0.0000	1.00	0.0073	0.0006	1.08
K35dn		0.0000	1.00		0.0000	1.00		0.0000	1.00		0.0000	1.00
K36up	0.0073	0.0000	1.00	0.0073	0.0000	1.00	0.0078	0.0000	1.00	0.0077	0.0000	1.00
K36dn		0.0000	1.00		0.0000	1.00		0.0000	1.00		0.0000	1.00

(Continued on following page)

TABLE 9 | (*Continued*) Required ductility values of the columns for the distributions of the horizontal loads.

	Initial design			Strengthened by							
				Code			min (CM-CR)			min (CM-CV)	
	θ_y	$\theta_{pl,dem}$	μ_{dem}	θ_y	$\theta_{pl,dem}$	μ_{dem}	θ_y	$\theta_{pl,dem}$	μ_{dem}	θ_y	$\theta_{pl,dem}$	μ_{dem}
K37up	0.0090	0.0000	1.00	0.0098	0.0000	1.00	0.0098	0.0000	1.00	0.0098	0.0000	1.00
K37dn		0.0000	1.00		0.0000	1.00		0.0000	1.00		0.0000	1.00
K38up	0.0090	0.0000	1.00	0.0090	0.0000	1.00	0.0081	0.0000	1.00	0.0085	0.0000	1.00
K38dn		0.0000	1.00		0.0000	1.00		0.0000	1.00		0.0000	1.00
μ	—	—	1.00	—	—	1.00	—	—	1.00	—	—	1.01
σ	—	—	0.00	—	—	0.00	—	—	0.00	—	—	0.02
CoV	—	—	0.00	—	—	0.00	—	—	0.00	—	—	0.02

design (**PP IN**), strengthened based on the design code (**PP DC**), strengthened based on minimum rigidity eccentricity (**PP CR**), and strengthened based on minimum strength eccentricity (**PP CV**).

Comparing the performance points (PPs) of the structural systems derived through the optimization process with the original one and the strengthened one based on the design code (Kanepe, 2017), the following observations can be stated: 1) the base shear value for PP was almost doubled for both new structural systems. 2) The deformation for PP was significantly reduced for almost all horizontal load combinations examined (by 25%–30%). These results were more or less expected because, as observed previously, the rigidity and bearing capacity of the two new structural systems increased significantly compared to the original and strengthened ones. However, it is worth noting that 3) both new structural systems derived are considered safe because no end of structural element exceeds the "life safety" performance level. The number of ends of columns that enter the plastic zone is reduced (limited to the bottom ends of the ground floor columns). However, the total number of edges of the structural elements that enter the plastic zone does not change substantially. This is due to increase of base shear. Thus, beams without being strengthened further take over larger forces, resulting in plasticized ends. Even so, no beam exceeded the "life safety" performance level.

5.4.3 Ductility Demand of the Columns

The view of the structure where deformation due to torsion is added to the one due to translational motion is called the "flexible view," while the view on which deformation due to torsion is subtracted due to translational motion is called "rigid view." It was observed through nonlinear static analyses that increased inelastic deformation is observed for the flexible side and reduced for the rigid in comparison to the corresponding deformation of symmetrical structural systems. Therefore, the unbalanced distribution of the ductility demand to eccentric buildings can lead to failures due to unexpected excitations (Stathopoulos and Anagnostopoulos, 2005; Anagnostopoulos et al., 2015). In this section, the distribution of ductility demand for the design earthquake will be measured for the columns of each floor for all four structural systems. In order to control the distribution of ductility demand, the coefficient of variation (*CoV*) will be used, which is a measure of the relative variability and measures the spread of the data in relation to the mean value defined as

$$CoV = \frac{StDev}{Mean} \tag{19}$$

where *StDev* is the standard deviation and *Mean* is the mean value of data. The ductility of beams or columns is defined as follows:

$$\mu_\theta = 1 + \frac{\theta_{pl}}{\theta_y}, \tag{20}$$

where θ_{pl} is the plastic rotation angle at the edges of the structural elements and θ_y is the yield rotation angle, both calculated based on Kanepe (2017). In order to calculate the required ductility, the value of θ_{pl}, for each edge of the column structural element for the design earthquake of EC8, is calculated. Based on the values of θ_{pl} and θ_y of the ends of the columns and using **Eq. 19**, **Table 9** is formed. Based on the results presented in **Table 9**, it can be observed that the distribution of ductility in the columns for the two optimization-based strengthening designs is more balanced in relation to the original structural system and the one strengthened based on the design goal B1 of Kanepe (2017), resulting into more controllable structural performance.

The ground floor is a representative story to identify changes in ductility distribution over the columns where plastic hinges are formed at the edges of all columns in each structural system. On the ground floor, it is observed that *CoV* of ductility demand decreases for the designs resulting from the optimization process. Thus, unbalanced distribution of ductility demand over the columns is mitigated. For the first story, in the case of the structural systems derived through the solution of the minimum stiffness and strength eccentricity problems due to higher stiffness, no plastic hinge was created, while for the second story where, as expected, due to the lowest stress intensity developed, none plastic hinge was formed in any of the four structural systems.

6 CONCLUSION AND DISCUSSION

In the present study, the aim was to minimize the torsional response of a multi-story reinforced concrete (RC) building by strengthening its columns. The ultimate goal was to improve its structural behavior

through an automized procedure that could be easily utilized in relevant structural analysis and design software. In this direction, design optimization problems were formulated based on the torsional response criterion. Therefore, the problem was mathematically developed with two independent formulations: minimization of the eccentricity between mass and rigidity centers and minimization of the eccentricity between mass and strength centers. The first one was formulated as a discrete structural optimization problem, where the dimensions of the columns' cross sections were the unknowns. In contrast, the second was formulated as a mixed one, where, in addition to the dimensions, the percentage of the reinforcement was the unknowns. The two problems were solved using the evolutionary algorithm called the imperialist competitive algorithm (ICA).

In the first part of the investigation, the case study building was assessed based on nonlinear static analyses aiming to assess its behavior for the case of the design earthquake. The nonlinear static analyses revealed that larger deformations are observed along the X direction. Subsequently, strengthening interventions were to be decided on some of the structural elements aiming to meet the B1 design goal of Kanepe (2017), that is, for the design seismic action, the structural system should not exceed the "life safety" performance level. Given that all structural elements were considered primary ones, none of them should exceed the specified performance level. In order to meet these needs, it was decided to strengthen column K7 using RC jacketing, resulting in the reduction of target deformation demands along the X direction, and no structural element of the structural system developed damage larger than the acceptable one for the design earthquake.

The next step, in terms of strengthening, used the optimization framework developed to minimize stiffness and strength eccentricities. By means of nonlinear static analyses performed for the two new structural systems resulting by solving the two optimization problems, it was found that the bearing capacity and stiffness almost doubled compared to the original and the strengthened ones based on Kanepe (2017), while their ductility was significantly increased. The deformation corresponding to the performance point was significantly reduced for almost all horizontal load combinations examined by 25%–30%. Due to the large increase in the base shear at the performance point, the number of plastic hinges at the ends of the beams was increased since the cross sections of the columns were strengthened. Even so, none beam exceeded the "life safety" performance level. These results were expected due to extensive strengthening of the columns. The main conclusion that emerged is that the distribution of ductility in the columns is more balanced in relation to the original structural system and the one strengthened based on the design goal B1 of Kanepe (2017).

DATA AVAILABILITY STATEMENT

The original contributions presented in the study are included in the article/Supplementary Material, Further inquiries can be directed to the corresponding author.

AUTHOR CONTRIBUTIONS

All authors have made a substantial, direct, and intellectual contribution to the work and approved it for publication.

FUNDING

The research was funded by the Hellenic Foundation for Research and Innovation (H.F.R.I.) under the "Second Call for H.F.R.I. Research Projects to support Post-Doctoral Researchers," IMSFARE project: "Advanced Information Modelling for SAFER Structures against Manmade Hazards" (Project Number: 00356).

REFERENCES

Almazán, J. L., and de la Llera, J. C. (2009). Torsional Balance as New Design Criterion for Asymmetric Structures with Energy Dissipation Devices. *Earthquake Engng Struct. Dyn.* 38 (12), 1421–1440. doi:10.1002/eqe.909

Anagnostopoulos, S. A., Kyrkos, M. T., and Stathopoulos, K. G. (2015). Earthquake Induced Torsion in Buildings: Critical Review and State of the Art. *Earthquakes and Structures* 8 (2), 305–377. doi:10.12989/eas.2015.8.2.305

Anastassiadis, K., Athanatopoulou, A., and Makarios, T. (1998). Equivalent Static Eccentricities in the Simplified Methods of Seismic Analysis of Buildings. *Earthquake Spectra* 14 (1), 1–34. doi:10.1193/1.1585986

Applied Technology Council (ATC) (1996). *Methodology for Evaluation and Upgrade of Reinforced concrete Buildings, Report N. ATC-40*. Sacramento, California: California Seismic Safety Commission.

Atashpaz-Gargari, E., and Lucas, C. (2007). Imperialist Competitive Algorithm: An Algorithm for Optimization Inspired by Imperialistic Competition. *IEEE Congress Evol. Comput.*, 4661–4667. doi:10.1109/CEC.2007.4425083

Bosco, M., Ferrara, G. A. F., Ghersi, A., Marino, E. M., and Rossi, P. P. (2015). Predicting Displacement Demand of Multi-Storey Asymmetric Buildings by Nonlinear Static Analysis and Corrective Eccentricities. *Eng. Structures* 99, 373–387. doi:10.1016/j.engstruct.2015.05.006

Bosco, M., Ghersi, A., and Marino, E. M. (2012). Corrective Eccentricities for Assessment by the Nonlinear Static Method of 3D Structures Subjected to Bidirectional Ground Motions. *Earthquake Engng Struct. Dyn.* 41 (13), 1751–1773. doi:10.1002/eqe.2155

Bosco, M., Marino, E. M., and Rossi, P. P. (2013). An Analytical Method for the Evaluation of the In-Plan Irregularity of Non-regularly Asymmetric Buildings. *Bull. Earthquake Eng.* 11 (5), 1423–1445. doi:10.1007/s10518-013-9438-3

Chandler, A. M., Correnza, J. C., and Hutchinson, G. L. (1995). Influence of Accidental Eccentricity on Inelastic Seismic Torsional Effects in Buildings. *Eng. Structures* 17 (3), 167–178. doi:10.1016/0141-0296(94)00003-c

Costa, A., Arêde, A., and Varum, H. (2017). *Strengthening and Retrofitting of Existing Structures (Building Pathology and Rehabilitation Book 9) Part of: Building Pathology and Rehabilitation (21 Books)*. Singapore: Springer.

Dang, Y., Zhao, G., Tian, H., and Li, G. (2021). Two-Stage Optimization Method for the Bearing Layout of Isolated Structure. *Adv. Civil Eng.* 2021, 1–10. art. No. 4895176. doi:10.1155/2021/4895176

De Stefano, M., and Pintucchi, B. (2008). A Review of Research on Seismic Behaviour of Irregular Building Structures since 2002. *Bull. Earthquake Eng.* 6 (2), 285–308. doi:10.1007/s10518-007-9052-3

Duan, X. N., and Chandler, A. M. (1997). An Optimized Procedure for Seismic Design of Torsionally Unbalanced Structures. *Earthquake Engng. Struct. Dyn.* 26 (7), 737–757. doi:10.1002/(sici)1096-9845(199707)26:7<737::aid-eqe673>3.0.co;2-s

Etedali, S., and Kareshk, M. K. (2022). Mitigation of Torsional Responses in Asymmetric Base-Isolated Structures Using an Optimal Distribution of Isolators in Base story. *Structures* 35, 807–817. doi:10.1016/j.istruc.2021.11.053

Eurocode 8 (1994). *European Committee for Standardization ENV 1998-1-1:1994. Design of Structures for Earthquake Resistance – Part 1: General Rules, Seismic Actions and Rules for Buildings*. Brussels, Belgium.

Eurocode 1 (1995). *European Committee for Standardization ENV 1991-1-1:1995. Actions on Structures – Part 1-1: General Actions – Densities, Selfweight, Imposed Loads for Buildings*. Brussels, Belgium.

Fajfar, P. (2000). A Nonlinear Analysis Method for Performance-Based Seismic Design. *Earthquake Spectra* 16 (3), 573–592. doi:10.1193/1.1586128

Fajfar, P., and Fischinger, M. (1988). Discussion of " Evaluation of Building Code Formulas for Earthquake Forces " by Anil K. Chopra and Ernesto F. Cruz (August 1986, Vol. 112, No. 8). *J. Struct. Eng.* 114 (3), 735–737. doi:10.1061/(asce)0733-9445(1988)114:3(735)

Fajfar, P., and Gašperšič, P. (1996). The N2 Method for the Seismic Damage Analysis of RC Buildings. *Earthquake Engng. Struct. Dyn.* 25 (1), 31–46. doi:10.1002/(sici)1096-9845(199601)25:1<31::aid-eqe534>3.0.co;2-v

Ganguly, K. K. (2020). *Reinforced Concrete Design: Repair/Restoration, Strengthening of RC Structures and Concrete Technology*. India: Medtech.

Georgoussis, G. K. (2015). Minimizing the Torsional Response of Inelastic Multistory Buildings with Simple Eccentricity. *Can. J. Civ. Eng.* 42 (11), 966–969. doi:10.1139/cjce-2015-0091

Goel, R. K., and Chopra, A. K. (1990). Inelastic Seismic Response of One-Storey, Asymmetric-Plan Systems: Effects of Stiffness and Strength Distribution. *Earthquake Engng. Struct. Dyn.* 19 (7), 949–970. doi:10.1002/eqe.4290190703

Guo, W., and Li, H.-N. (2009). Secondary System's Optimal Position Analysis Concerning the Lateral-Torsion Coupling Effect. *Jisuan Lixue Xuebao/Chinese J. Comput. Mech.* 26 (6), 797–803+810. doi:10.1088/0256-307x/26/7/074218

Hejal, R., and Chopra, A. K. (1989). Earthquake Response of Torsionally Coupled, Frame Buildings. *J. Struct. Eng.* 115, 834. doi:10.1061/(asce)0733-9445(1989)115:4(834)

Humar, J. L. (1984). Design for Seismic Torsional Forces. *Can. J. Civ. Eng.* 11 (2), 150–163. doi:10.1139/l84-027

Ismail, M. (2015). Elimination of Torsion and Pounding of Isolated Asymmetric Structures under Near-Fault Ground Motions. *Struct. Control. Health Monit.* 22 (11), 1295–1324. doi:10.1002/stc.1746

Kan, C. L., and Chopra, A. K. (1977). Effects of Torsional Coupling on Earthquake Forces in Buildings. *J. Struct. Div.* 103 (4), 805–819. doi:10.1061/jsdeag.0004608

Kanepe (2017). *Earthquake Planning & Protection Organization (EPPO). Greek Code for Assessment and Retrofitting*. 2nd revision(in Greek). Athens, Greece.

Lagaros, N. D., Bakas, N., and Papadrakakis, M. (2009). Optimum Design Approaches for Improving the Seismic Performance of 3D RC Buildings. *J. Earthquake Eng.* 13 (3), 345–363. doi:10.1080/13632460802598594

Lagaros, N. D., Papadrakakis, M., and Bakas, N. (2006). Automatic Minimization of the Rigidity Eccentricity of 3D Reinforced concrete Buildings. *J. Earthquake Eng.* 10 (4), 533–564. doi:10.1080/13632460609350609

Lagaros, N. D., Plevris, V., and Kallioras, N. Ath. (2022). *The Mosaic of Metaheuristic Algorithms in Structural Optimization*. Archives of Computational Methods in Engineering. (to appear).

Li, C.-X., and Han, C.-F. (2003). Optimum Placements of Multiple Tuned Mass Dampers (MTMD) for Suppressing Torsional Vibration of Asymmetric Structures. *J. Earthquake Eng. Eng. Vibration* 23 (6), 149–155.

Li, C.-X., Qu, Y., Wang, C., and Li, J.-H. (2008a). Characteristics of a Soil-Asymmetric Building-Active Tuned Mass Damper Interaction System. *Zhendong yu Chongji/Journal of Vibration and Shock* 27 (9), 26–31.

Li, C.-X., Qu, Y., Wang, C., and Li, J.-H. (2008b). Optimum Properties of Soil-Asymmetric Building-Amtmd Interaction System. *Zhendong yu Chongji/Journal of Vibration and Shock* 27 (10), 10–14.

Li, C.-X., Xu, Z.-M., and Zhang, L.-Q. (2008c). Earthquake Reduction Behaviors of Active Tuned Mass Dampers for an Asymmetric Building. *Zhendong yu Chongji/Journal of Vibration and Shock* 27 (1), 76–83+88.

Makarios, T., and Anastassiadis, K. (1998). Real and Fictitious Elastic Axes of Multi-Storey Buildings: Theory. *Struct. Des. Tall Build.* 7 (1), 33–55. doi:10.1002/(sici)1099-1794(199803)7:1<33::aid-tal95>3.0.co;2-d

Maruić, D., and Fajfar, P. (2005). On the Inelastic Seismic Response of Asymmetric Buildings under Bi-axial Excitation. *Earthquake Engng Struct. Dyn.* 34 (8), 943–963. doi:10.1002/eqe.463

Palermo, M., Silvestri, S., Gasparini, G., and Trombetti, T. (2017). A Comprehensive Study on the Seismic Response of One-Storey Asymmetric Systems. *Bull. Earthquake Eng.* 15 (4), 1497–1517. doi:10.1007/s10518-016-0030-5

Palermo, M., Silvestri, S., Gasparini, G., and Trombetti, T. (2013). Physically-based Prediction of the Maximum Corner Displacement Magnification of One-Storey Eccentric Systems. *Bull. Earthquake Eng.* 11 (5), 1467–1491. doi:10.1007/s10518-013-9445-4

Papazachos, B. C., Papaioannou, C. A., Margaris, B. N., and Theodulidis, N. P. (1993). Regionalization of Seismic hazard in Greece Based on Seismic Sources. *Nat. Hazards* 8 (1), 1–18. doi:10.1007/bf00596232

Paulay, T. (1998). Torsional Mechanisms in Ductile Building Systems. *Earthquake Engng. Struct. Dyn.* 27, 1101–1121. doi:10.1002/(sici)1096-9845(199810)27:10<1101::aid-eqe773>3.0.co;2-9

Penelis, G., and Penelis, G. (2019). *Concrete Buildings in Seismic Regions*. United States: CRC Press.

Peruš, I., and Fajfar, P. (2005). On the Inelastic Torsional Response of Single-Storey Structures under Bi-axial Excitation. *Earthquake Engng Struct. Dyn.* 34 (8), 931–941. doi:10.1002/eqe.462

Reem, H., and Chopra, A. K. (1987). *Earthquake Response of Torsionally-Coupled Buildings, Earthquake Engineering Research Center*. Berkeley: College of Engineering: University of California at Berkeley.

Şahin, A. (2012). A New Algorithm for Geometrical Design of Asymmetric Tall Buildings against Seismic Torsional Behaviour. *Struct. Des. Tall Spec. Build.* 21 (9), 642–668. doi:10.1002/tal.634

Stathi, C. G., Bakas, N. P., Lagaros, N. D., and Papadrakakis, M. (2015). Ratio of Torsion (ROT): An index for Assessing the Global Induced Torsion in Plan Irregular Buildings. *Earthquakes and Structures* 9 (No. 1), 145–171. doi:10.12989/eas.2015.9.1.145

Stathopoulos, K. G., and Anagnostopoulos, S. A. (2005). Inelastic Torsion of Multistorey Buildings under Earthquake Excitations. *Earthquake Engng Struct. Dyn.* 34, 1449–1465. doi:10.1002/eqe.486

Tassios, T. P. (1982). *The Mechanics of Column Repair with a Reinforced concrete Jacket*. Athens, Greece: 7th European Conference on Earthquake Engineering ECEE.

Terzi, V. G., and Athanatopoulou, A. (2021). Optimum Torsion axis in Multistory Buildings under Earthquake Excitation: A New Criterion Based on axis of Twist. *Eng. Structures* 249, 113356. doi:10.1016/j.engstruct.2021.113356

Trombetti, T. L., and Conte, J. P. (2005). New Insight into and Simplified Approach to Seismic Analysis of Torsionally Coupled one-story, Elastic Systems. *J. Sound Vibration* 286 (1-2), 265–312. doi:10.1016/j.jsv.2004.10.021

Xenidis, H., Makarios, T., and Athanatopoulou, A. (2006). The Properties of the Optimum Torsion axis in Asymmetric Multi-Storey Buildings. *Technica Chronica, Sci. J. Tcg*, 99–112.

Yiu, C.-F., Chan, C.-M., Huang, M., and Li, G. (2014). Evaluation of Lateral-Torsional Coupling in Earthquake Response of Asymmetric Multistory Buildings. *Struct. Des. Tall Spec. Build.* 23 (13), 1007–1026. doi:10.1002/tal.1102

Author's Disclaimer: The content of this paper expresses the views of the authors and not the official position of the Ministry of Maritime Affairs and Insular Policy.

Conflict of Interest: The authors declare that the research was conducted in the absence of any commercial or financial relationships that could be construed as a potential conflict of interest.

Publisher's Note: All claims expressed in this article are solely those of the authors and do not necessarily represent those of their affiliated organizations or those of the publisher, the editors, and the reviewers. Any product that may be evaluated in this article, or claim that may be made by its manufacturer, is not guaranteed or endorsed by the publisher.